Investigating neutrino oscillation experiments - A study of some aspects of T2K and Super–Kamiokande Photo Multiplier Tubes Technologies

A report submitted in partial fulfillment of the requirements for
the award of the degree of

M.Sc. Physics

by

REVATHY N

MYAMWPH012

Department of Physics
Mercy College, Palakkad, 678 006
2024

Investigating neutrino oscillation experiments - A study of some aspects of T2K and Super–Kamiokande Photo Multiplier Tubes Technologies

A report submitted to the University of Calicut in partial fulfillment of
the requirements for
the award of the degree of

M.Sc. Physics

by

REVATHY N

MYAMWPH012

CERTIFIED AS BONAFIED RESEARCH WORK

External Examiner:

1:＿＿＿＿＿＿＿＿＿   HOD

2:＿＿＿＿＿＿＿＿＿   Internal Examiner

Candidate's Declaration

I hereby certify that the work, which is being presented in the project report, titled **Investigating neutrino oscillation experiments - A study of some aspects of T2K and Super–Kamiokande Photo Multiplier Tubes Technologies**, in partial fulfillment of the requirement for the award of the Degree of Master of Science and submitted to the institution is an authentic record of my own work carried out during the period **Jan-2024 to May-2024** under the supervision of **Dr. Lakshmi .S. Mohan**. I have also cited the references for the sources of the text(s)/figure(s)/table(s)/equation(s) wherever required.

The matter presented in this report has not been submitted elsewhere for the award of any other degree or diploma from any institutions.

Date: _____

Signature of the Candidate

Certificate

This is to certify that the work titled **Investigating neutrino oscillation experiments - A study of some aspects of T2K and Super–Kamiokande Photo Multiplier Tubes Technologies**, carried out by **REVATHY N**, in partial fulfillment of the requirement for the award of the Degree of Master of Science and submitted to the institution is an authentic work under the the guidance of Dr. Lakshmi .S. Mohan, Post Doctoral Fellow, University of Silesia in Katowice, Poland. The work presented in this thesis has not been submitted for the award of any degree or diploma earlier.

Signature of research supervisor(s)   **Signature of Head of the Department**

Dr. Lakshmi .S. Mohan   Dr. Lakshmi. M

Post Doctoral Fellow   Asst.Professor

University of Silesia in Katowice, Poland   Mercy College Palakkad

Acknowledgements

I would like to express my first and foremost gratitude to my guide Dr. Lakshmi. S. Mohan for her immense support and guidance. Words feel much shorter for me to convey how thankful I am to do my project under her. Despite being in different time zones, she scheduled and adjusted time for me and my doubts, corrected my mistakes and made me to be the better of myself, I believe that I met your standard to some extend.

This project couldn't be possible without KTPI, Kerala Theoretical Physics Initiative. I would like to thank all the members of KTPI for giving me such an opportunity and to work under Lakshmi ma'am.

I would like this opportunity to express my gratitude to my class tutor, mentor and one of my greatest supporter Dr. Anu. S. Kuruvila for her immense support and the belief she has in me.

Thank you, Akshara P, without your presence and mutual motivation, completion of this project wouldn't be the same.

My heartfelt gratitude to a bunch of girls, my friends for their support and making me believe that I can do more. I extend my gratitude to all other teaching and non–teaching staffs of my college.

I am nothing without my family, I would like to thank all my family members, especially all the women in my family in believing in me, and for never giving up in their respective lives.

Lastly, I am thankful to my god, who always make me believe in a strong positive aura.

Abstract

Neutrino oscillations, a phenomenon where neutrinos change their flavor as they propagate from one point to the other, provides crucial information about their nature and can also provide information about our universe. Tokai 2 Kamioka (T2K) is a long base–line accelerator neutrino experiment designed to study these oscillations with high precision. This project gives a short description of the experimental setup and working of T2K and studies some aspects of the experiment in detail. Since T2K was the first experiment to implement the *off–axis* beam technique, the first aim of this project is to study the off-axis beam technique in detail, which produces a narrow band neutrino beam from the 2–body decay of charged pions in flight into (anti–)muon and muon (anti–)neutrino. From the study of the kinematics of this decay process it is understood that the energy of the neutrino depends on the energy of the charged pions and the angle at which the neutrino is emitted w.r.to the parent pion direction in the lab frame. The relative neutrino flux is also studied. The second study of this thesis focuses on an aspect of the far detector of the T2K, Super–Kamiokande (SK). The Cherenkov radiation produced by the final state particles from a neutrino interaction in SK is detected by the Photo Multiplier Tubes (PMTs) present in the inner–walls of SK detector. The important outputs from a PMT are the charge and timing infomrations. The charge is proportional to the number of electrons collected at the PMT anode and provide the collectible electric signals corresponding to the detection of a neutrino. The variation of anode electron distribution for different PMT parameters are studied in detail. This information is crucial in the simulation studies of the a detector which uses PMTs as active detectors. Thus two different aspects of T2K experiment were studied and understood.

Contents

List of Figures

List of Tables

CHAPTER 1

Introduction

The study of neutrino and its properties plays an important role in understanding the vast universe still unknown to humankind. Neutrino is an electrically neutral particle with a tiny but finite mass, which interacts via weak and gravitational interactions only. The neutrino was first proposed by Wolfgang Pauli in 1930[19] as a solution to the β–decay anomaly [20]. This was a major breakthrough since this could solve the problem of energy–momentum conservation in *beta*–decay which was considered to be a 2–body decay at that time.

The observations showed that the electron spectrum was continuous as shown in Fig. 1.1, which would not have been, had β–decay been a 2–body decay process. Pauli
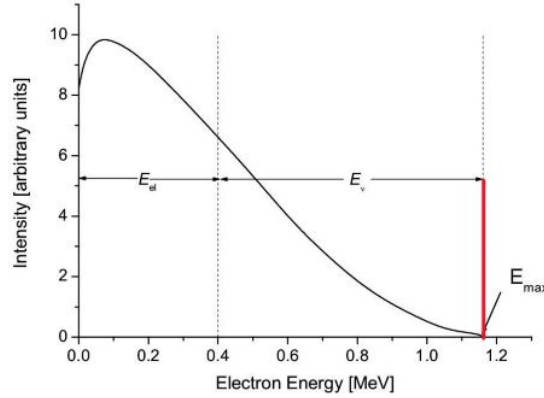
Figure 1.1: Electron energy vs intensity of the β spectrum. The expected electron energy is shown in red [1].

proposed that β–decay is a 3–body decay process where neutrinos were emitted along with the other particles. Then the processes could be written as:

$$n \longrightarrow p + e^- + \overline{\nu}_e \qquad ; \qquad p \longrightarrow n + e^+ + \nu_e \tag{1.1}$$

He theorized that the new particles were chargeless and massless with $\frac{1}{2}$ spin [20].

1.1 Fermi theory and neutrino

In 1934 a quantitative theory of β emission, in which neutrino was incorporated, was proposed by Enrico Fermi [21]. The neutrino (ν) was assumed to be neutral, with a mass $\leq$ mass of electron. In a β decay process, a detectable electron and an escaping neutrino are emitted simultaneously, where the neutrino carries part of the energy.

As shown in Eqn. 1.1, a neutron in the nucleus decays into a proton, simultaneously creating an electron and a neutrino, via weak interaction which is weaker than the electromagnetic force. Fermi explained that this neutrino carries away some part of the kinetic energy (from energy–momentum conservation), thus giving rise to the continuous electron spectrum. This solved the conservation of energy. Because of the success of Fermi's theory, almost all scientists of the time believed that neutrino could exist. But the direct detection of neutrinos was possible only in 1956 [22].

1.2 Experimental discovery of neutrino

With Fermi's theory of weak force it was possible to consider the inverse β–decay reaction,

$$\overline{\nu}_e + p \longrightarrow n + e^+ \tag{1.2}$$

But the weak force is so weak that the probability of inverse β– decay was calculated to be ≈ 0. Since the weak interaction cross sections are so small in target materials, the detection of neutrinos could take place only with the advent of intense neutrino sources and development of further detection technologies. The detection of $\overline{\nu}_e$ was first done in the Savannah River experiment in 1956 [23] by Fredrick Reines and Clyde Cowan. They used a nuclear reactor as an intense source of $\overline{\nu}_e$ and detected it using inverse β– decay process shown in Eqn. 1.2. They had first conducted their experiment Project Poltergeist [24] at the Hanford site and obtained some preliminary results. But the definitive experiment was conducted in early 1956 at P Reactor (where the $\overline{\nu}_e$ flux was of the order of 10^{13} $cm^{-2}s^{-1}$) at the Savannah River Plant with a better cosmic ray shielding [23].

The principle of detection used in this experiment is explained briefly here. Electron anti–neutrinos ($\overline{\nu}_e$) are produced in the fission processes in a nuclear reactor. These $\overline{\nu}_e$ would interact with the protons present in the water target with scintillator and cadmium chloride ($CdCl_2$) dissolved in it. The positron e^+ emitted in this reaction will annihilate with e^- in the meidum and produce two γ rays, which travel in opposite directions.

$$e^+ + e^- \longrightarrow \gamma + \gamma \tag{1.3}$$

Each γ has an energy of 511 keV and the two γ rays are detected by two large scintillation detectors on the opposite sides of the target, in coincidence. To be sure that it was indeed $\overline{\nu}_e$ that interacted in the detector, it was necessary to detect the neutron also produced in the interaction. These neutrons can be captured on hydrogen in the detector, but elements like Cadmium have a higher capture cross section for low energy neutrons. When a neutron is absorbed by Cd, ^{108}Cd produces an excited state of ^{109}Cd which subsequently emits a gamma ray of energy ≈ 9 MeV.

$$n + {}^{108}\text{Cd} \longrightarrow {}^{109}\text{Cd}^* \longrightarrow {}^{108}\text{Cd} + \gamma \tag{1.4}$$

The two γs from annihilation and the single γ from the de–excitation of ^{109}Cd* should have a delayed coincidence of 5 μs. The schematic of the detector setup is shown in Fig. 1.2.

About 3 $\overline{\nu}_e$ per hour were detected with a source about 11 m from the detector. Data was taken after switching off the reactor to ensure that $\overline{\nu}_e$ were indeed detected when the reactor was on.
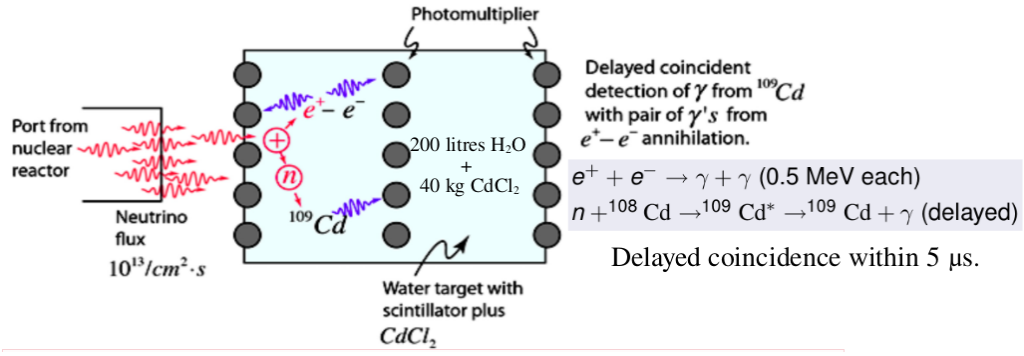
Figure 1.2: The schematic diagram showing the $\bar{\nu}_e$ detection process in the Savannah river experiment[2].

1.3 The Standard Model of elementary particles

The Standard Model (SM) [25] illustrated in Fig. 1.3 is a theoretical framework for elementary particles and their interactions.
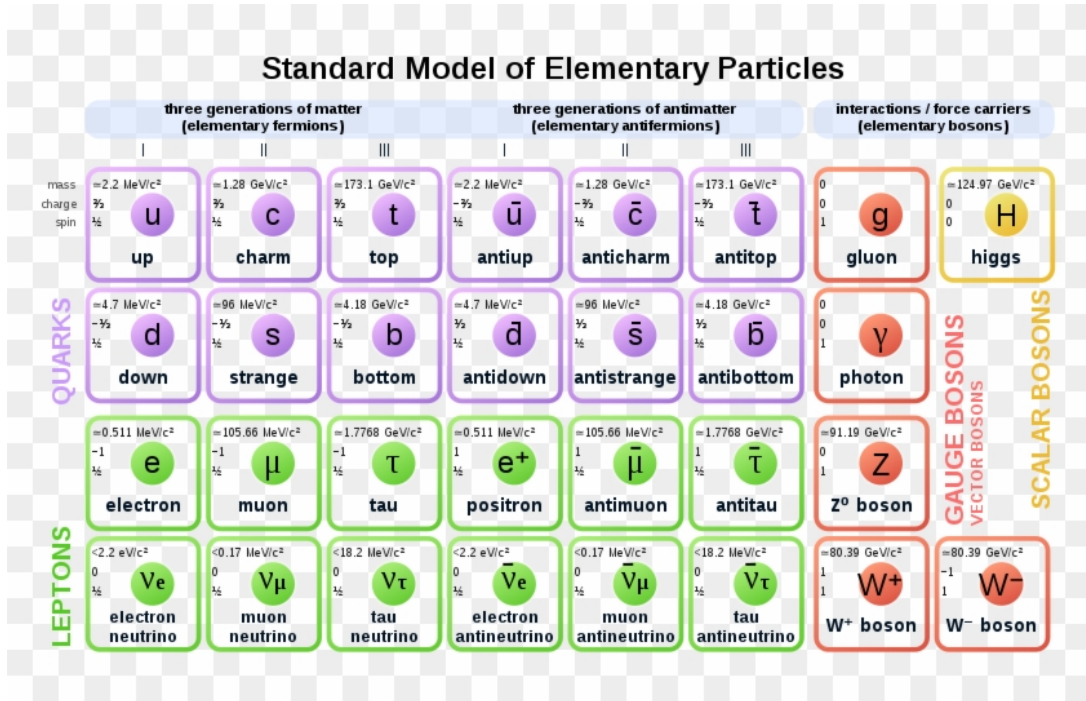
Figure 1.3: Standard Model of elementary particles [3].

It contains fermions (with half–integer spins) and bosons (with integer spins) [26, 27, 28] – i.e the elementary particles and the force carriers between them. There are two types of fermions namely *quarks* and *leptons* characterised by their mass, charge, spin and interactions [29]. There are four types of interactions which the particles experience, namely strong, weak, electromagnetic and gravity.

Quarks [1] participate in all four interactions, where as charged leptons like electron participate in all interactions expect strong interactions. Neutrinos interact only via weak and gravitational interactions since they are neutral leptons. All fermions have

---

[1] Quarks are the elementary components of hadrons but do not exist has free particles.

their respective anti–particles with the same mass but opposite charge. The masses and charges of quarks and leptons are listed in Fig. 1.3.

The four fundamental interactions are mediated by their own force carrying bosons. Photons mediate the electromagnetic interactions, gluons mediate the strong interactions, the $W^{\pm}$ and Z^0 bosons mediate weak interactions. Photons and gluons are massless, while $W^{\pm}$ and Z^0 are massive particles. Gravity is said to be mediated by gravitons. The relative strength of the fundamental interactions are given in Table. 1.1.

Force	Relative strength	Range
Strong	1	$< 10^{-15}$ m
Electromagnetic	10^{-2}	∞
Weak	10^{-3}	10^{-15} m
Gravitational	10^{-39}	∞

Table 1.1: The relative strength and range of fundamental forces [17].

In the standard model, neutrinos are considered to be massless for all practical purposes. But the discovery of neutrino oscillations is evidence that neutrinos have a tiny but finite masses [30]. This is a very important discovery which was awarded the Nobel Prize in Physics in 2015 [30].

1.4 Sources of neutrinos

Neutrinos are produced in different sources in the universe. Generally, neutrino sources can be divided into two categories: (i) **natural** and (ii) **human/machine made**. All these sources which emit neutrinos at different energies are described in detail here.

1.4.1 Natural Sources

Natural sources of neutrinos emit neutrinos of different energies depending on the neutrino production mechanisms. The main natural sources of neutrinos are:

- **Cosmological neutrinos:**

  The standard Big Bang cosmology predicts the existence of a, relic Cosmic Neutrino Background (CNB) similar to the Cosmic Micorwave Background (of photons) (CMB). These are neutrinos, which got decoupled from thermodynamical equilibrium in the early universe after Big Bang, are the second most abundant particles in the universe (the first being photons) with a density of ~ 330 cm^{-3}. The current temperature of these neutrinos is ~ 1.95 K which is equivalent to an energy of 2×10^{-4} eV [31].

- **Solar neutrinos:**

  In Sun, the main energy generating mechanism is the fusion of hydrogen to helium. There are two main thermonuclear reactions in the solar core which produce energy and neutrinos, namely *p–p chain* and *CNO–cycle* as shown in Fig. 1.4.
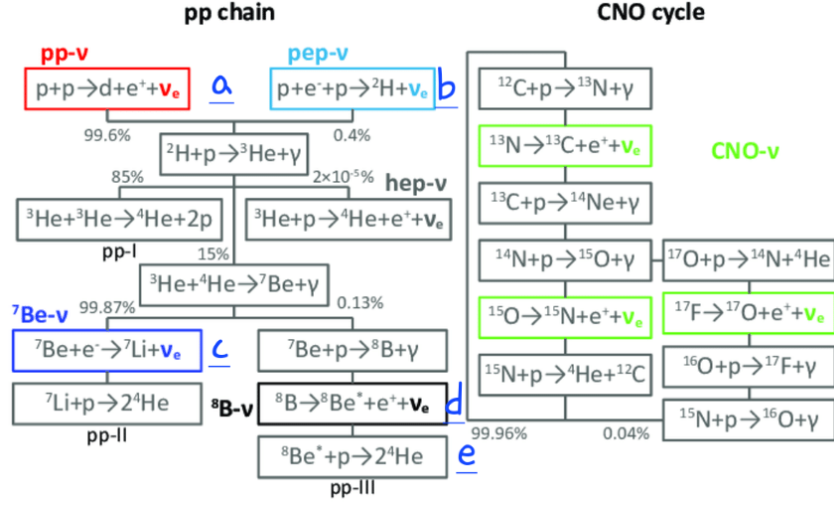
Figure 1.4: Solar neutrino production via p–p chain and CNO cycle [4].

Reaction	Energy of neutrino E_ν(MeV)
(a) $p + p \rightarrow d + e^+ + \nu_e$	< 0.42
(b) $p + e^- + p \rightarrow d + \nu_e$	1.44
(c) $e^- + {}^7\text{Be} \rightarrow {}^7\text{Li} + \nu_e$	$0.86(90\%), 0.38\ (10\%)$
(d) ${}^8\text{B} \rightarrow {}^8\text{Be}^* + \text{e}^- + \nu_\text{e}$	< 15
(e) ${}^3\text{He} + p \rightarrow {}^4\text{He} + e^+ + \nu_e$	< 18.8

Table 1.2: The energy range of neutrino produced in the processes of p–p chain only [18]. The labels (a), (b), (c), (d) and (e) are marked in Fig. 1.4.

14

The expected flux of solar neutrino on the Earth's surface as a function of neutrino energy is shown in Fig. 1.5. The total flux is $\sim 6.5 \times 10^{10} cm^{-2} s^{-1}$ [18]. The discovery of solar neutrinos were awarded the 2002 Physics Nobel Prize [32].
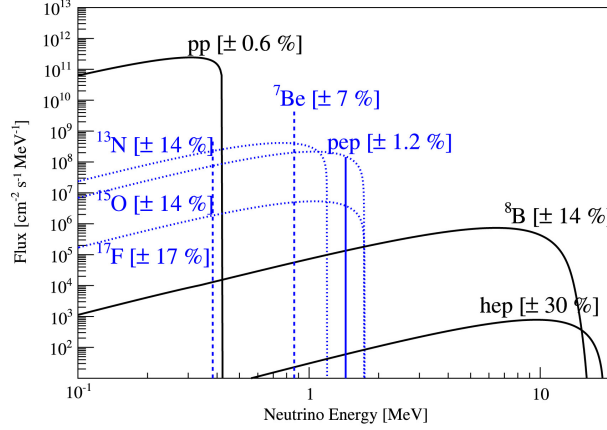
Figure 1.5: Neutrino fluxes (with percentage uncertainties), predicted by the Bahcall–Serenelli solar model (BS05)[5], in $cm^{-2} s^{-1} MeV^{-1} (cm^{-2} s^{-1}$ for the lines).

- **Supernova neutrinos:**

  The collapse of the core of massive stars produce large fluxes of neutrinos that could be detected on the Earth. Stars with masses $> 10 M_\odot$, where $M_\odot$ is the solar mass, undergo nuclear fusion of H, He, C, O, Ne, Si until they have an onion–like structure, with an Fe core surrounded by shells composed of elements with decreasing atomic mass. This iron core has a mass of about $1 M_\odot$, radius of a few 1000 km, a central density of $\sim 10^{10} gm\ cm^3$, a central temperature of ~ 1 MeV and its weight is sustained by the pressure of degenerate relativistic electrons. Iron being the most tightly bound nucleus, further thermonuclear fusions will not occur. The contraction of the core causes an increase in temperature resulting in the photo–dissociation of iron through

  $$\gamma + {}^{56}Fe \longrightarrow 13 {}^4He + 4 {}^1n. \tag{1.5}$$
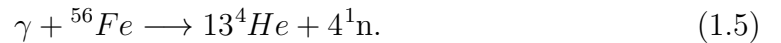
  About 124 MeV of energy is absorbed by this reaction reducing the kinetic energy and pressure of the electrons. Electron capture of nuclei and free proton,

  $$e^- + (Z, A) \longrightarrow (Z-1, A) + \nu_e$$
  $$e^- + p \longrightarrow n + \nu_e \tag{1.6}$$
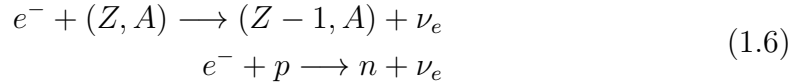
  The neutrinos have an average energy of 12–16 MeV. Neutrinos of all flavors are produced in the hot core of the proto–neutron star through pair production:

  $$e^+ + e^- \longrightarrow \nu_a + \overline{\nu}_a \tag{1.7}$$

  where $a = e, \mu, \tau$.

  Electron capture processes also produce ν_e and positron capture on neutrons produce $\bar{\nu}_e$. Since all flavors of (anti–)neutrino are produced during SN, the energy range is ~ 10–20 MeV. Neutrinos from SN 1987A were detected in Kamiokande and other experiments like IMB, on 24 February 1987 [33]. This SN occured in the Large Magellanic Cloud, located at a distance of ~ 50 kpc from the solar system. The discovery was awarded the Nobel Physics Prize of 2002 [32].

15

- **Geo neutrinos:**

  These are $\bar{\nu}_e$ that come from radioactive decays of unstable isotopes in the Earth's interior. Their sources are natural β^- decays of nuclides including ^{238}U & ^{232}Th families and ^{40}K.

  $$^{238}\text{U} \longrightarrow {}^{206}\text{Pb} + 8\,^4\text{He} + 8e^- + 6\bar{\nu}_e + 51.7 MeV \tag{1.8}$$

  $$^{232}\text{Th} \longrightarrow {}^{208}\text{Pb} + 6\,^4\text{He} + 4e^- + 4\bar{\nu}_e + 42.7 MeV \tag{1.9}$$

  $$^{40}\text{K} \longrightarrow {}^{40}\text{Ca} + e^- + 1.31 MeV \tag{1.10}$$

  Though the geo–neutrino flux at Earth's surface is $\sim 10^6 \; cm^{-2}s^{-1}$, their detection is challenging.

- **Atmospheric neutrinos:**

  Atmospheric neutrinos are created the following processes [34]. Primary cosmic rays composed of protons, alpha particles, heavier nuclei along with small quantities of electrons interact with the nuclei in the upper atmosphere to generate secondary cosmic rays. Secondary cosmic rays include hadrons, mainly charged pions and their decay products, with an energy spectrum peaking in the GeV range and extending to higher energies. The pions decay according to the decay chain

  $$\pi^+ \longrightarrow \mu^+ + \nu_\mu \quad ; \quad \pi^- \longrightarrow \mu^- + \bar{\nu}_\mu. \tag{1.11}$$

  The resulting $\mu^\pm$ decay according to

  $$\mu^+ \longrightarrow e^+ + \nu_e + \bar{\nu}_\mu \quad ; \quad \mu^- \longrightarrow e^- + \bar{\nu}_e + \nu_\mu. \tag{1.12}$$

  These neutrinos are called atmospheric neutrinos and their energies range from ~ 0.1–100 GeV. In atmospheric neutrinos, there are 2 mu–like neutrinos produced for every e–like neurtrino (summed over both neutrinos and anti–neutrinos). Atmospheric neutrino detectors are usually kept underground (or have a rock overburden) to filter out the secondary cosmic ray muon background, which will mimic neutrino interactions in the same energy range in a detector.

- **Astrophysical neutrinos:**

  High energy neutrinos of PeV – TeV energies can travel through interstellar media, without getting deflected by magnetic fields. This enables the probing of high energy phenomena of the universe, leading to tests of particle interactions and fundamental laws [35]. In 2013 IceCube neutrino observatory reported the first detection of extraterrestrial neutrinos with energies between 10 TeV and 2 PeV [36]. Icecube has observed about 80 neutrino events with deposited energies from 20 TeV to 2 PeV [36].

1.4.2 Artificial neutrino sources

Neutrinos of different energies are also produced in the lab. The main artificial sources of neutrinos are described here.

- **Reactor anti–neutrinos:**

  Nuclear reactors are the strongest source of terrestrial anti–neutrinos. The β–decay of unstable fissile isotopes like ^{238}U and ^{239}Pu produce $\bar{\nu}_e$ flavour, since Eqn. 1.1 is the underlying process. The energies of reactor $\bar{\nu}_e$ peak around 3 MeV and extend up to about 8 MeV [37] [38].

- **Accelerator neutrinos:**

  Accelerator neutrino production is similar to that of atmospheric neutrinos but the processes happen in a controlled environment. A high energy proton beam impinges a thick nuclear target, producing secondary charged pions and kaons, which leave the target, boosted in the forward direction but with some divergence given by production cross section. The mesons decay in flight to (anti-)neutrinos. The interaction producing $\pi^{\pm}$ and $K^{\pm}$ are

$$p + {}^{12}\text{C} \longrightarrow \pi^{\pm} + X \quad ; \quad p + {}^{12}\text{C} \longrightarrow K^{+}(K^{-}) + X \tag{1.13}$$

The mesons decay in flight as

$$\begin{aligned} \pi^{+} &\longrightarrow \mu^{+} + \nu_{\mu} \quad ; \quad \pi^{-} \longrightarrow \mu^{-} + \overline{\nu}_{\mu} \\ K^{+} &\longrightarrow \mu^{+} + \nu_{\mu} \quad ; \quad K^{-} \longrightarrow \mu^{-} + \overline{\nu}_{\mu}. \end{aligned} \tag{1.14}$$

The charged mesons are focussed using magnetic horns so that either π^{+} or K^{+} (π^{-} or K^{-}) decay inside the decay volume giving a predominantly ν_{μ} ($\bar{\nu}_{\mu}$) beam with less backgrounds. Accelerator neutrinos are unidirectional and can tuned to a specific energy range depending on the oscillation experiment. For T2K experiment E_{ν} peaks at 0.6 GeV with a narrow band of energies[39][40]. The NOνA uses a beam, which peaks at ~ 2.0 GeV[41].

The measured and expected fluxes of (anti–)neutrinos from natural and artificial sources are shown in Fig. 1.6 [6]. Different sources emit neutrinos of different energies. To detect neutrinos in different energy ranges, different detector technologies are employed.
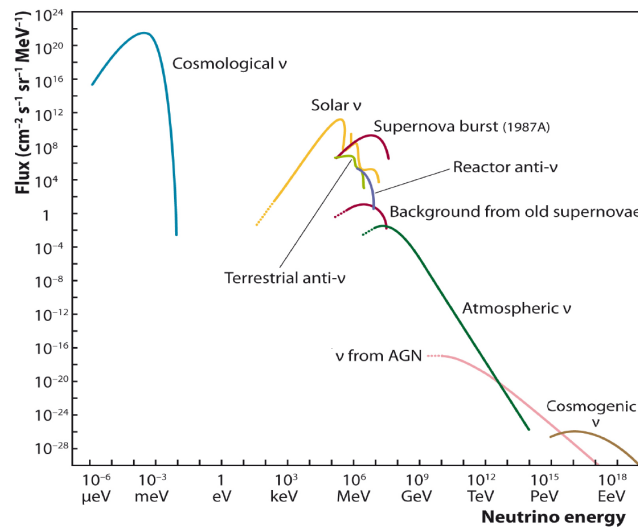
Figure 1.6: Measured and predicted fluxes of neutrinos from different sources as a function of neutrino energy [6].

1.5   Neutrino oscillations in vacuum

In section 1.3 we saw that the neutrino were assumed to be massless in the Standard Model. The discovery of the phenomenon of neutrino oscillations in solar and atmospheric neutrinos by SNO and Super–Kamiokande established the existence of neutrino oscillations [42, 43]. The phenomenon where a flavour ν_α ($\bar{\nu}_\alpha$) changes to another flavour ν_β ($\bar{\nu}_\beta$) after travelling a distance L is called *neutrino oscillations*. Since oscillations occur, neutrinos should have a tiny but finite mass and physics beyond Standard model should exist.

Neutrino oscillation is a quantum mechanical phenomenon, theory of neutrino oscillations in vacuum is explained briefly here. The flavour eigen states ν_α (where $\alpha = e, \mu, \tau$) which we produce and detect via experiments, are superpositions of different mass eigen states ν_i (where i = 1,2,3). i.e a flavour ν_α created with a momentum p can be written as:

$$|\nu_\alpha\rangle = \sum_k U_{\alpha k}^* |,\nu_k\rangle \qquad (1.15)$$

where $U_{\alpha k}^*$ is the element of the unitary mixing matrix. Consider a finite normalization volume V, such that the mass neutrino states are orthonormal:

$$\langle \nu_k | \nu_j \rangle = \delta_{kj} \qquad (1.16)$$

Since the mixing matrix U is unitary, the flavour states are also orthonormal:

$$\langle \nu_\alpha | \nu_\beta \rangle = \delta_{\alpha\beta} \qquad (1.17)$$

The massive neutrino states $|\nu_k\rangle$ are eigenstates of the Hamiltonian ,

$$\mathbf{H}|\nu_k\rangle = E_k|\nu_k\rangle \qquad (1.18)$$

where E_k are the energy eigenvalues given by

$$E_k = \sqrt{\vec{p}^2 + m_k^2}, \qquad (1.19)$$

where m_k is the mass of $|\nu_k\rangle$. Since the Schrodinger equation has the form,

$$i\frac{d}{dt}|\nu_k(t)\rangle = \mathbf{H}|\nu_k(t)\rangle \qquad (1.20)$$

the massive neutrino states evolve in time as plane waves given by

$$|\nu_k(t)\rangle = e^{-iE_k t}|\nu_k\rangle. \qquad (1.21)$$

Let $\nu_\alpha(t)$ be a flavor state describing a neutrino created with a definite flavor α at time $t = 0$. From Eqns. 1.15 and 1.21, the time evolution of $\nu_\alpha(t)$ is given by

$$|\nu_\alpha(t)\rangle = \sum_k U_{\alpha k}^* e^{-iE_k t}|\nu_k\rangle. \qquad (1.22)$$

such that

$$|\nu_\alpha(t = 0)\rangle = |\nu_\alpha\rangle \qquad (1.23)$$

Using the unitarity relation

$$U^\dagger U = 1,$$

$$\sum_i U_{\alpha i} U^*_{\beta i} = \delta_{\alpha\beta} \tag{1.24}$$

So $|\nu_k\rangle$ is given by

$$|\nu_k\rangle = \sum_\alpha U_{\alpha k} |\nu_\alpha\rangle. \tag{1.25}$$

By substitution of Eqn. 1.25 into Eqn. 1.22,

$$|\nu_\alpha(t)\rangle = \sum_{\beta=e,\mu,\tau} \left(\sum_k U^*_{\alpha k} e^{-iE_k t} U_{\beta k} \right) |\nu_\beta\rangle. \tag{1.26}$$

The coefficient of $|\nu_\beta$

$$A_{\nu_\alpha \to \nu_\beta}(t) \equiv \langle \nu_\beta | \nu_\alpha(t) \rangle = \sum_k U^*_{\alpha k} U_{\beta k} e^{-iE_k t} \tag{1.27}$$

is the amplitude of $\nu_\alpha \to \nu_\beta$ transitions as a function of time. The probability of transition is

$$P_{\nu_\alpha \to \nu_\beta}(t) = |A_{\nu_\alpha \to \nu_\beta}(t)|^2 = \sum_{k,j} U^*_{\alpha k} U_{\beta k} U_{\alpha j} U^*_{\beta j} e^{-i(E_k - E_j)t}. \tag{1.28}$$

For ultra–relativistic neutrinos,

$$E_k \simeq E + \frac{m_k^2}{2E} \tag{1.29}$$

Therefore,

$$E_k - E_j \approx \frac{\Delta m_{kj}^2}{2E}, \tag{1.30}$$

where

$$\Delta m_{kj}^2 = m_k^2 - m_j^2 \tag{1.31}$$

is the mass squared difference and

$$E = |\vec{p}| \tag{1.32}$$

is the neutrino energy for $m_\nu \approx 0$. Therefore, the transition probability in eqn 1.28 can be approximated by

$$P_{\nu_\alpha \to \nu_\beta}(t) = \sum_{k,j} U^*_{\alpha k} U_{\beta k} U_{\alpha j} U^*_{\beta j} \, exp\left(-i \frac{\Delta m_{kj}^2 t}{2E} \right) \tag{1.33}$$

In an actual neutrino oscillation experiment, the propagation time t is not measured, but distance L between the source and the detector is known. Ultra–relativistic neutrinos propagate with $v \approx c$, and $c = 1$ in natural units, $t = L$. So $P_{\nu_\alpha \to \nu_\beta}(t)$ becomes

$$P_{\nu_\alpha \to \nu_\beta}(L, E) = \sum_{k,j} U^*_{\alpha k} U_{\beta k} U_{\alpha j} U^*_{\beta j} \, exp\left(-i \frac{\Delta m_{kj}^2 L}{2E} \right). \tag{1.34}$$

The quartic products containing the elements of the mixing matrix U determine the amplitude of oscillations whereas the term

$$\Phi_{k,j} = -\frac{\Delta m_{kj}^2 L}{2E} \tag{1.35}$$

determines the phase of oscillations. Thus the measurement of neutrino oscillations allow us to determine the values of Δm_{kj}^2 and elements of U.

Transitions among different flavors occur for $L > 0$. Because the unitarity relation,

$$UU^\dagger = 1 \iff \sum_k U_{\alpha k} U_{\beta k}^* = \delta_{\alpha\beta}, \tag{1.36}$$

$$P_{\nu_\alpha \to \nu_\beta}(L = 0, E) = \delta_{\alpha\beta}. \tag{1.37}$$

Then the probability in Eqn. 1.34 can be written as

$$P_{\nu_\alpha \to \nu_\beta}(L, E) = \sum_k |U_{\alpha k}|^2 |U_{\beta k}|^2 + 2Re \sum_{k>j} U_{\alpha k}^* U_{\beta k} U_{\alpha j} U_{\beta j}^* exp\left(-2\pi i \frac{L}{L_{kj}^{osc}}\right), \tag{1.38}$$

with the constant and oscillating terms are separated and the oscillation length is defined as the distance at which the phase generated by Δm_{kj}^2 becomes equal to 2π :

$$L_{kj}^{osc} = \frac{4\pi E}{\Delta m_{kj}^2}. \tag{1.39}$$

Oscillation probability in Eqn. 1.34 can be rewritten by separating the real and imaginary parts of the quartic products of U elements. From the square of the unitary relation in Eqn. 1.36,

$$\sum_k |U_{\alpha k}|^2 |U_{\beta k}|^2 = \delta_{ab} - 2\sum_{k>j} Re\left(U_{\alpha k}^* U_{\beta k} U_{\alpha j} U_{\beta j}^*\right). \tag{1.40}$$

Then after some simplifications the neutrino oscillation probability can be written as

$$
\begin{aligned}
P_{\nu_\alpha \to \nu_\beta}(L, E) = \delta_{ab} &- 4\sum_{k>j} Re\left(U_{\alpha k}^* U_{\beta k} U_{\alpha j} U_{\beta j}^*\right) \sin^2\left(\frac{\Delta m_{kj}^2 L}{4E}\right) \\
&+ 2\sum_{k>j} Im\left(U_{\alpha k}^* U_{\beta k} U_{\alpha j} U_{\beta j}^*\right) \sin\left(\frac{\Delta m_{kj}^2 L}{2E}\right)
\end{aligned} \tag{1.41}
$$

The probability is called *transition probability* when $\alpha \neq \beta$ and is called *survival probability* when $\alpha = \beta$.

For an anti–neutrino, flavour $|\overline{\nu_\alpha}\rangle$

$$|\overline{\nu_\alpha}\rangle = \sum_k U_{\alpha k} |\overline{\nu_k}\rangle \tag{1.42}$$

And following the steps as in the neutrino case, the probability of oscillation of $\bar{\nu}_\alpha \to \bar{\nu}_\beta$ is given by:

$$
\begin{aligned}
P_{\bar{\nu}_\alpha \to \bar{\nu}_\beta}(L, E) = \delta_{\alpha\beta} &- 4\sum_{k>j} Re\left(U_{\alpha k}^* U_{\beta k} U_{\alpha j} U_{\beta j}^*\right) \sin^2\left(\frac{\Delta m_{kj}^2 L}{4E}\right) \\
&- 2\sum_{k>j} Im\left(U_{\alpha k}^* U_{\beta k} U_{\alpha j} U_{\beta j}^*\right) \sin\left(\frac{\Delta m_{kj}^2 L}{2E}\right)
\end{aligned} \tag{1.43}
$$

The difference between the ν and $\bar{\nu}$ oscillation probabilities in vacuum is the sign of the imaginary terms in Eqn. 1.41 and Eqn. 1.43.

Since we have 3 active (anti–)neutrino flavours ν_α ($\bar{\nu}_\alpha$), where $\alpha = e, \mu, \tau$, the mixing matrix is a 3×3, unitary matrix named the U_{PMNS} matrix. $U = U_{PMNS}$ for three neutrino mixing and oscillations is [44]:

$$U = \begin{pmatrix} c_{12}c_{13} & s_{12}c_{13} & s_{13}e^{-i\delta} \\ -s_{12}c_{23} - c_{12}s_{23}s_{13}e^{i\delta} & c_{12}c_{23} - s_{12}s_{23}s_{13}e^{i\delta} & s_{23}c_{13} \\ s_{12}s_{23} - c_{12}c_{23}s_{13}e^{i\delta} & -c_{12}s_{23} - s_{12}c_{23}s_{13}e^{i\delta} & c_{23}c_{13} \end{pmatrix} \tag{1.44}$$

where $c_{ij} = \cos\theta_{ij}$, $s_{ij} = \sin\theta_{ij}$ (where i, j = 1,2,3) and δ is the Dirac CP phase.

1.6 Neutrino Oscillation Experiments

Experiments which use neutrinos from several sources have confirmed the phenomenon of oscillations. Some of the important sources and the (anti–)neutrino flavours from them are listed in Table. 1.3:

Source	ν or $\bar{\nu}$ flavours produced	Neutrino energy (E)
Nuclear power plants	$\overline{\nu}_e$	$3 - 8$ (MeV)
The Sun	ν_e	$0.1 - 20$ (MeV)
Particle accelerators	$\nu_e, \nu_\mu, \overline{\nu}_e, \overline{\nu}_\mu$	> 0.1 (GeV)
Earth's atmosphere	$\nu_e, \nu_\mu, \overline{\nu}_e, \overline{\nu}_\mu$	$0.1 - 100$ (GeV)

Table 1.3: Some of the important neutrino sources with the flavours and energies of (anti–)neutrinos emitted from them. Experiments which detected these neutrinos gave us experimental evidence for the phenomenon of neutrino oscillations.

The neutrino oscillation experiments are of two types, **short–baseline** and **long–baseline**. Of these, accelerator long baseline (LBL) experiments are relevant for this. There are several LBL experiments worldwide, which have either finished running (K2K [45], MINOS [46]), currently taking data (T2K[39],[40], NOνA [41]) and are being built (T2HK [47], DUNE [48]). These experiments are sensitive to the oscillation parameters in the 2–3 sector and the Dirac CP phase δ_{CP}. A brief discussion about some of the main LBL experiments are presented here.

– **MINOS:**
  (Main Injectior Neutrino Oscillation Search) experiment used NuMI (Neutrino at Main Injector) beam which provided an intense beam of ν_μ of energies in

the few GeV range, with a peak at 3 GeV. MINOS had near and far detectors, the near detector situated at Fermilab, 1.02 km from the target, measured the energy spectra of the ν before oscillation. The magnetised far detector located at the Soudan Underground Laboratory in northern Minnesota, 705 m underground and 735 km from the target, measured the oscillated neutrino spectra and saw the appearance and disappearance of neutrinos due to oscillation. The experiment measured θ_{23} and $|\Delta m^2_{32(1)}|$ and finished operation on June 29, 2016.

– **NOVA**:

(NuMi Off-axis electron Neutrino Appearance) experiment also uses NUMI beam to observe $\nu_\mu(\overline{\nu}_\mu) \to \nu_e(\overline{\nu}_e)$ appearance and $\nu_\mu(\overline{\nu}_\mu) \to \nu_\mu(\overline{\nu}_\mu)$ disappearance in oscillation. This experiment also has a near and far detector, the former is located 100 m underground, about 1 km from the production point ad the latter is located at Ash river, Minneosota, $\sim$ 810 km from the source. Both detectors receive a narrow band neutrino flux peaking at 1.8 GeV with an off–axis angle (technique discussed in chapter. 3) of 14.6 mrad (0.8°) and neutrino energy within 1.0 – 5.0 GeV. NOνA also measures the 2–3 oscillation parameters and δ_{CP}.

– T2K : Tokai 2 Kamioka (T2K) experiment is currently running and will be discussed in detail in chapter. 2.

1.7 Scope of this thesis

Accelerator long baseline (LBL) experiments are an imporant class of neutrino oscillation experiments trying to understand the fundamental nature of neutrinos. One of the main LBL experiments running currently is T2K, which makes use of an off–axis technique to generate a narrow band neutrino beam. The far detector of T2K is Super–Kamiokande which uses Photo Multiplier Tubes (PMTs) to detect the cherenkov light produced in particle interactions. In this thesis I have studied these two aspects. Chapter 2 gives a brief description of T2K experiment including its near and far detectors. The off–axis technique is studied in chapter 3. The kinematics of 2–body decay in flight and the dependence of neutrino energy on the pion energy and off–axis angle are studied. The calculation of the energy–angle spectrum of neutrinos also is done. The aspects of PMTs and the variation of their responses with different parameters are studied in chapter 4. These studies are relevant for the simulations of detectors involving photo multiplier tubes. The summary and future plans are described in chapter. 5.

CHAPTER 2

T2K experiment

Tokai 2 Kamioka (T2K) experiment, is one of the important accelerator long base-line neutrino oscillation experiments. It mainly studies the disappearance of ν_μ ($\bar{\nu}_\mu$) and appearance of ν_e ($\bar{\nu}_e$) from a predominantly ν_μ ($\bar{\nu}_\mu$) beam [49]. It measures the neutrino oscillation parameters $\theta_{23}, \Delta m^2{}_{32}$ and δ_{CP} and neutrino–nucleus interaction cross sections. The experiment has a baseline of 295 km over which neutrino oscillation takes place. It has near and far detector components which measure the neutrinos before and after the oscillations take place.

The ν_μ ($\bar{\nu}_\mu$) beam is produced by the decay of π^+ (π^-). The proton beam to produce the pion beam is provided by Japan Proton Accelerator Research complex (J–PARC) [50], situated at Tokai on the east coast of Japan. T2K experiment has near and far detector complexes. The near detector complex has an on–axis detector INGRID and an off–axis detector ND280 situated at a distance of 280 m from the target. The far detector is Super–Kamiokande [51] which is situated at a distance of 295 km from the target.

2.1 T2K experiment – short description

A short description of T2K experiment with its schematic is given in this section. The schematic of T2K is shown in Fig. 2.1.

A protom beam of kinetic energy 30 GeV produced in J–PARC is directed towards a graphite target where hadrons (mostly pions) are produced in the proton–carbon interactions. The target region is followed by a 110 m long decay volume filled with with Helium gas in which charged pions and kaons decay in flight to muons and muon-neutrinos. The secondary $\pi^+(-)$ (and kaons) from the target are focused by three electromagnetic horns operated at a (-)250 kA pulsed current. Depending on the polarity of the current either π^+ is focused or π^- is focused. Operation in the
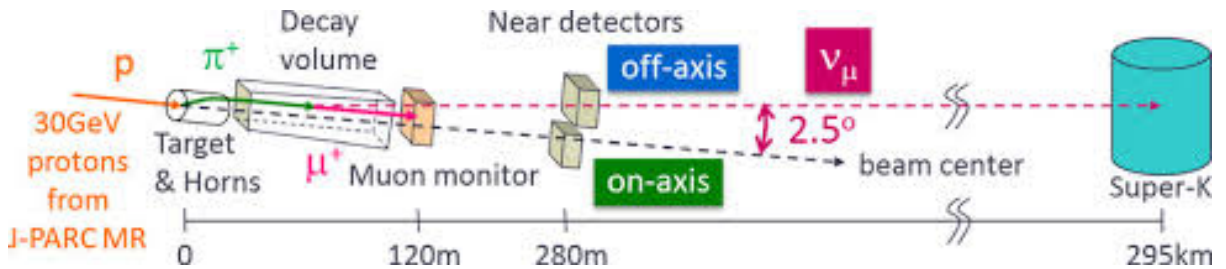
Figure 2.1: Schematic of T2K experiment [7].

forward horn current (FHC) mode produces a predominantly neutrino beam and the operation in the reverse horm current (RHC) mode produces a predominantly anti–neutrino beam. The beam dump, consisting of graphite blocks ~ 3.15 m thick, followed by iron plates ~ 2.5 m thick in total, is placed downstream at the end of the decay volume.A muon monitor (MUMON) is placed just behind the beam dump to monitor the intensity and profiles of muons, which pass through beam dump on a spill–by–spill basis.

The (anti–)neutrino beam is allowed to pass through the near detector complex ND280 and INGRID (shown in Fig. 2.2) located at 280 m from the target to constrain the measurments of neutrino fluxes and cross sections off–axis and on–axis respectively. The measurement of the oscillated (anti–)neutrino beam is done by Super–Kamiokande (SK) situated off–axis at a distance of 295 km from the target.
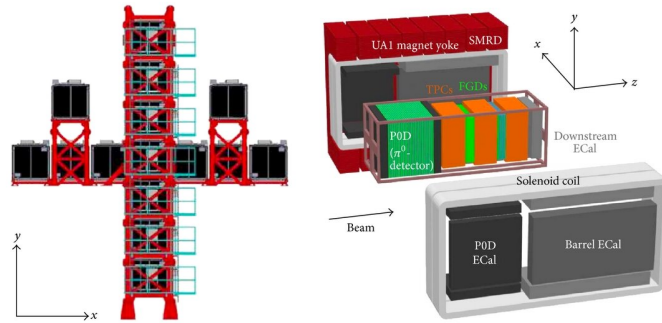
Figure 2.2: The on-axis detector INGRID and the off-axis detector ND280.
[52]

T2K is the first experiment to employ the "off–axis" technique which is discussed detail in 3. Both ND280 and SK are situated at an off–axis angle of 2.5°. Consequently, the neutrino beam passing through Super–Kamiokande has a narrow energy spectrum ranging from 0.2–2.0 GeV with a peak around ~ 0.6 GeV where the oscillation maximum for 295 km occurs as illustrated in Fig. 2.3. This technique enhances the monochromatic character of the ν_μ ($\overline{\nu}_\mu$) beam produced. A high–intensity, highly collimated beam with the a narrow energy spectrum is obtained as a result.

N280 provides the constraint on neutrino cross sections where as some constraints on fluxes are obtained from INGRID. The oscillated events in SK provide the constraints on oscillation parameters. The most significant measurements from T2K are the first indication and later confirmation of ν_e ($\overline{\nu}_e$) appearance in a ν_μ ($\overline{\nu}_\mu$) beam[53], the most precise measurement of the θ_{23} parameter[54]. The first significant constraint on the δ_{CP} parameter, responsible for the matter–antimatter asymmetry in the neutrino oscillations[53] was also obtained from the T2K's measurements.

2.2 Far detector: Super–Kamiokande

The far detector of T2K is Super–Kamiokande (Super–K, SK), which measures neutrino interaction rate after oscillations. Super–K also functions as an independent detector and detects atmospheric neutrinos[55] and neutrinos from other sources such are the Sun [56] and is looking for supernova neutrinos. Half of the 2015
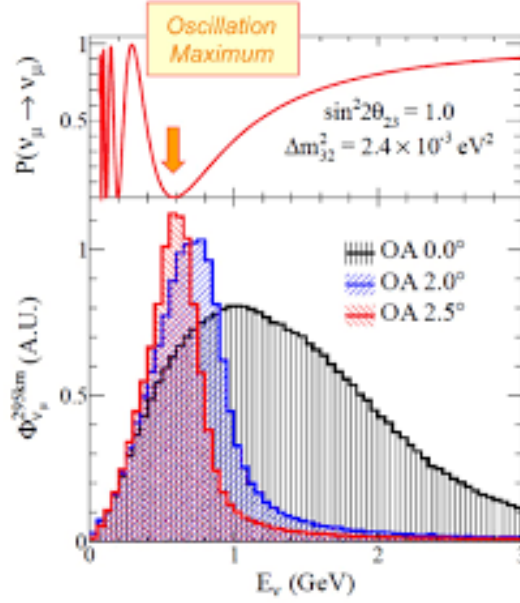
Figure 2.3: Neutrino off–axis flux and approximate probability of the ν_μ disappearance at the far detector [8].

Nobel Physics Prize was for the discovery of atmospheric neutrino oscillations by Super–K [30]. It was also an integral for the accelerator experiment K2K[45].

Super–K is a large water Cherenkov detector located 1 km under Mt. Ikenoyama, near Kamioka on the west coast of Japan. The detector is a large cylinderical tank filled with 50 kton water and divided optically into an inner detector (ID) and an outer detector (OD). The inner wall of ID has 11146 PMTs, which cover 40% of the surface [51]. The wall is also covered with special coating to prevent light reflecting back into the ID volume. The OD is only sparsely instrumented and it is covered with 1885 outward facing PMTs. The purpose of the ID is to count a number of ν_μ and ν_e interactions to determine neutrino beam flavor composition and compare the results with the prediction from the ND280 and flux simulation. The OD removes the cosmic ray muons reaching the detector. The schematic of Super–K is shown in Fig. 2.4.
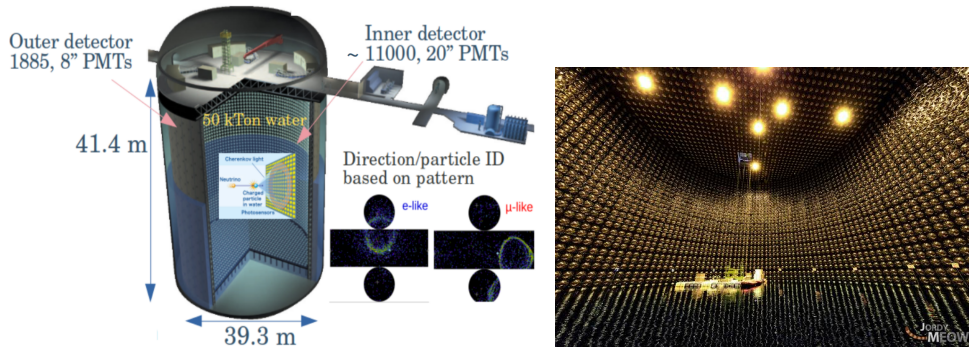
Figure 2.4: (Left) Schematic of Super–K. The inner and outer detectors which are optically separated from each other are shown. (Right) A view of SK from the inside while the tank was open, showing the PMTs on the inner detector wall.[9]

Super–K detects the neutrinos by means of Cherenkov radiation produced when
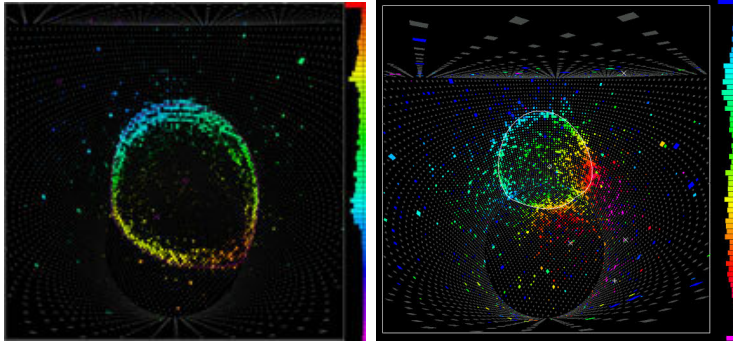
Figure 2.5: Muon–like and electron–like cherenkov rings formed in SK. Figure is from [10]

charged particles travel in a medium with a velocity $>$ the velocity of light in that medium. Charged current quasi–elastic interactions (CCQE) of ν_μ produces μ which appear as single ring events at T2K energies in SK. When leptons pass through water, they experience multiple Coulomb scattering. Since muons are $\sim$ 210 times heavier than the electrons, the electrons scatter more resulting in a diffuse ring where as muons have sharper rings as shown in Fig. 2.5.

Two different aspects of T2K experiment are studied in detail in this thesis. The chapter 3 deals with the off–axis beam technique which includes finding the energy of the neutrino, in relation with the parent pion energy and off–axis neutrino angle. The energy–angle spectrum of the neutrino flux is also studied. The chapter 4 deals with the Monte Carlo simulations of the anode electron distributions at PMTs which is relevant for the study of responses of PMTs in the far detector Super–K.

CHAPTER 3

Off–Axis Beam Technique

In the chapter 3 we discussed briefly discussed about T2K experiment. There the off–axis technique was mentioned along with the fact that ND280 and Super–K are situated at an off–axis angle of 2.5° from the proton target. The off–axis neutrino beam can be runed to be narrow and to peak at energies corresponding to oscillation maxima. Before we understand the off–axis technique it is important to understand the kinematics of 2–body decay of a particle in flight, since the charged pions in flight are decaying to produce the neutrino beam.

3.1 Relativistic Kinematics

Before understanding the details of 2–body decay of $\pi^{\pm}$ in flight, we need to understand the basics of relativistic kinematics starting with the space–time components.

3.1.1 Four–Vectors and Four–momentum

In the case of the Newtonian mechanics[1], an inertial frame is a frame in which the Newton's first law is valid and we consider space and time are treated independently. But for relativistic particles, space and time cannot be treated independently.

Hence in relativistic mechanics[2] we use a 4–vector, a vector having four components.

4–vector

The position–time 4–vector is x_{ν} where $\nu = 0, 1, 2, 3$:

$$x^0 = ct, x^1 = x, x^2 = y, x^3 = z [57] \tag{3.1}$$

$$X = (x^0, x^1, x^2, x^3) \equiv (ct, x, y, z) \equiv (x^0, \mathbf{r}) \tag{3.2}$$

The vector X in the Eqn. 3.2 is a contra–variant vector, where x^0 is the temporal and x^i $i = 1, 2, 3$ are the spatial components.

Similar to the 4–vector, we can define the 4–momentum p^{μ}

$$p^{\mu} = m\eta^{\mu}, \tag{3.3}$$

---

[1]The mechanics that deals with the concepts of Newton's law of motion, distance and velocity.

[2]Relativistic Mechanics deals with the mechanics of objects moving comparable to the speed of light

where

$$\eta^\mu = (\eta^0, \eta^1, \eta^2, \eta^3) = \gamma_\nu (c, v_x, v_y, v_z)$$

$$\gamma_\nu = \frac{1}{\sqrt{1 - \dfrac{v^2}{c^2}}}. \tag{3.4}$$

The components of p^μ

$$p^\mu = (p^0, p^1, p^2, p^3) = (E/c, p_x, p_y, p_z), \tag{3.5}$$

where E is the energy of the particle and is given by the relation $E^2 = m^2 c^4 + \vec{p}^2 c^2$.

4–Momentum

The components of the 4–momentum p^μ can be written from Eqns. 3.32 and 3.4
The temporal component is,

$$p^0 = \gamma mc \tag{3.6}$$

and the 3–momenta is

$$\vec{p} = \gamma m \vec{v}, \tag{3.7}$$

where γ is defined in Eqn. 3.4.
The relativistic energy is defined as

$$E = \gamma mc^2 \tag{3.8}$$

Since the temporal component of η is $\eta^0 = \gamma c$ then the the zeroth component of 4–momentum will be, $p^0 = E/c$. Thus the energy and the momentum will set up a new quantity called energy–momentum four–vector or simply four–momentum[57].

$$p^\mu = \left(\frac{E}{c}, p_x, p_y, p_z \right) \tag{3.9}$$

Square of the quantity η^μ is given by

$$\eta^\mu \eta_\mu = \gamma^2 \left(c^2 - v_x^2 - v_y^2 - v_z^2 \right) = \gamma^2 c^2 \left(1 - \frac{v^2}{c^2} \right) = c^2 \quad [57] \tag{3.10}$$

similarly we can find

$$p^\mu p_\mu = \frac{E^2}{c^2} - \vec{p}^2 = m^2 c^2 \quad [57]. \tag{3.11}$$

Then the 4–momentum is also invariant.

Lorentz Transformation and 4–vector

Lorentz transformation is a translation and/or rotation of the 4–vector space—time coordinate system relative to a fixed origin. Let there be a general transformation Λ^μ_ν of the co–ordinates from one inertial frame to the other

$$x^{\mu\prime} = \sum_{\nu=0}^{3} \Lambda^\mu_\nu x^\nu \tag{3.12}$$

$(\mu, \nu = 0, 1, 2, 3)$ x^μ is a contravariant vector. Using Einstein's summation convention, Eqn. 3.12 can be written as:

$$x^{\mu\prime} = \Lambda^\mu_\nu x^\nu \tag{3.13}$$

Though the coordinates of an event change according to Eqn. 3.13 when we go from one inertial frame (S) to the other (S') the following quantity remains *invariant* [57]:

$$ds^2 = (x^0)^2 - (x^1)^2 - (x^2)^2 - (x^3)^2 = (x^{0\prime})^2 - (x^{1\prime})^2 - (x^{2\prime})^2 - (x^{3\prime})^2. \tag{3.14}$$

Lorentz Boost

Boost is a special case of a Lorentz transformation.If the components of a 4–vector are measured in one frame, their values in another frame which is rotated or moving relative to the first can be found using Lorentz transformations. [58]. We can write

$$\gamma = \frac{1}{\sqrt{1 - \dfrac{v_x^2 + v_y^2 + v_z^2}{c^2}}} \tag{3.15}$$

$\beta_x = v_x/c$, $\beta_y = v_y/c$, $\beta_z = v_z/c$ where v_x, v_y and v_z are the velocities in the x, y and z directions respectively; c is the velocity of light in vacuum. The general matrix form of Lorentz boost is:

$$L = \begin{pmatrix} L_{tt} & L_{tx} & L_{ty} & L_{tz} \\ L_{xt} & L_{xx} & L_{xy} & L_{xz} \\ L_{yt} & L_{yx} & L_{yy} & L_{yz} \\ L_{zt} & L_{zx} & L_{zy} & L_{zz} \end{pmatrix}. \tag{3.16}$$

From Eqn. 3.16

$$L_{tt} = \gamma \tag{3.17}$$

$$L_{ta} = L_{at} = -\beta_a \gamma \tag{3.18}$$

$$L_{ab} = L_{ba} = (\gamma - 1)\{\frac{\beta_a \beta_b}{\beta_x^2 + \beta_y^2 + \beta_z^2}\} + \delta_{ab} \tag{3.19}$$

where $a, b, c = x, y, z$ and δ_{ab} is the Dirac delta function :

$$\delta_{ab} = 0 \quad \text{when} \quad a \neq b$$
$$= 1 \quad \text{when} \quad a = b.$$

Substituting the components of velocity in Eqn. 3.15 we get,

$$\gamma - 1 = \frac{1}{\sqrt{1 - (\beta_x^2 + \beta_y^2 + \beta_z^2)}} - 1. \tag{3.20}$$

Using binomial expansion,

$$(\gamma - 1) \approx \frac{1}{2} \left[\beta_x^2 + \beta_y^2 + \beta_z^2 \right] = \frac{v^2}{2c^2}. \tag{3.21}$$

Substituting for β_a and β_b we get

$$L_{ab} = L_{ba} = (\gamma - 1) \left(\frac{v_a v_b}{v^2} \right) + \delta_{ab}, \tag{3.22}$$

where,

$$v^2 = v_x^2 + v_y^2 + v_z^2$$

and

$$\gamma = \frac{1}{\sqrt{1 - \dfrac{v^2}{c^2}}}.$$

Substituting Eqn. 3.21 in Eqn. 3.22

$$L_{ab} = L_{ba} \approx \frac{\beta_a \beta_b}{2} \tag{3.23}$$

Then the matrix L becomes,

$$L = \begin{pmatrix} \gamma & -\beta_a a & -\beta_b b & -\beta_c c \\ -\beta_a a & \frac{\beta_a^2}{2} & \frac{\beta_a \beta_b}{2} & \frac{\beta_a \beta_c}{2} \\ -\beta_b b & \frac{\beta_a \beta_b}{2} & \frac{\beta_b^2}{2} & \frac{\beta_b \beta_c}{2} \\ -\beta_c c & \frac{\beta_a \beta_c}{2} & \frac{\beta_b \beta_c}{2} & \frac{\beta_c^2}{2} \end{pmatrix} \tag{3.24}$$

3.1.2 Lorentz transformations for a specific direction

So far we have discussed the Lorentz boost in general. Let us now consider two frames S and S', where S is fixed and S' is moving in the $+x$ direction with a velocity $+v$.

The Lorentz transformation from S to S' is given by:

$$X' = LX, \text{ where,} \tag{3.25}$$

$$X = \begin{pmatrix} x^0 \\ x^2 \\ x^2 \\ x^3 \end{pmatrix} = \begin{pmatrix} ct \\ x \\ y \\ z \end{pmatrix} \text{ and } X' = \begin{pmatrix} x^{0\prime} \\ x^{1\prime} \\ x^{2\prime} \\ x^{3\prime} \end{pmatrix} = \begin{pmatrix} ct' \\ x' \\ y' \\ z' \end{pmatrix} \tag{3.26}$$
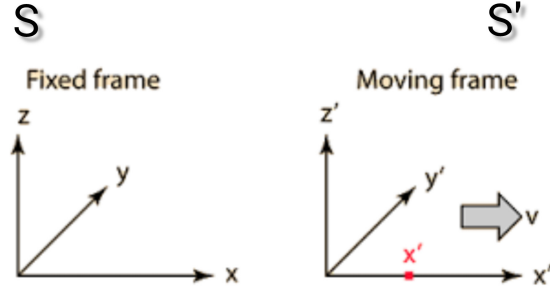
Figure 3.1: Lorentz Boost along x-axis with a velocity v[11]

.

The matrix L for this case is given by :

$$
L = \begin{pmatrix}
\gamma & -\beta\gamma & 0 & 0 \\
-\beta\gamma & \gamma & 0 & 0 \\
0 & 0 & 1 & 0 \\
0 & 0 & 0 & 1
\end{pmatrix}
\tag{3.27}
$$

Substituting Eqns. 3.27 and 3.26 in 3.25 gives

$$
\begin{pmatrix}
x^{0\prime} \\
x^{1\prime} \\
x^{2\prime} \\
x^{3\prime}
\end{pmatrix}
=
\begin{pmatrix}
\gamma x^0 + (-\beta\gamma)x^1 + 0 + 0 \\
(-\beta\gamma x^0 + \gamma)x^1 + 0 + 0 \\
0 + 0 + x^2 + 0 \\
0 + 0 + 0 + x^3
\end{pmatrix}
=
\begin{pmatrix}
\gamma x^0 - \beta\gamma x^1 \\
-\beta\gamma x^0 + \gamma x^1 \\
x^2 \\
x^3
\end{pmatrix}
\tag{3.28}
$$

Then for a Lorentz Boost along x–axis, the transformations from S to S' coordinates are:

$$
\begin{aligned}
x^{0\prime} &= \gamma x^0 - \beta\gamma x^1 \\
x^{1\prime} &= \gamma x^1 - \beta\gamma x^0 \\
x^{2\prime} &= x^2 \\
x^{3\prime} &= x^3
\end{aligned}
\tag{3.29}
$$

Similarly the transforms for the boost along y–direction are:

$$x^{0\prime} = \gamma x^0 - \beta\gamma x^1$$
$$x'^1 = x^1$$
$$x'^2 = \gamma x^2 - \beta\gamma x^0 \tag{3.30}$$
$$x'^3 = x^3$$

and those for boost along z direction will be:

$$x'^0 = \gamma x^0 - \beta\gamma x^1$$
$$x'^1 = x^1$$
$$x'^2 = x^2 \tag{3.31}$$
$$x'^3 = \gamma x^3 - \beta\gamma x^0$$

3.1.3   Lorentz transformation of 4-momentum components

The Lorentz boost in the $+z$ direction involves transforming the four-momentum of a particle. The four-momentum is transformed according to the Lorentz transformation matrix for a boost along the z-axis. The momentum should be considered as a four–vector then:

$$p^\mu = m\eta^\nu = (p^0, p^1, p^2, p^3), \tag{3.32}$$

where m is the mass of the particle and η^ν is the proper velocity. The Lorentz transformation matrix Λ^μ_ν, for a boost along the z direction [3] with a velocity v and $\beta = v/c$ where c is the velocity of light in vacuum and $\gamma = \dfrac{1}{\sqrt{1 - \dfrac{v^2}{c^2}}}$ is given as:

$$\Lambda^\mu_\nu = \begin{pmatrix} \gamma & 0 & 0 & -\beta\gamma \\ 0 & 1 & 0 & 0 \\ 0 & 0 & 1 & 0 \\ -\beta\gamma & 0 & 0 & \gamma \end{pmatrix} \tag{3.33}$$

Then the transformation of p^μ to p'^μ

$$p'^\mu = \Lambda^\mu_\nu p^\mu \tag{3.34}$$

Then the components of the transformed four–momentum are:

$$p'^0 = \gamma p^0 - \gamma\beta p^3$$
$$p'^1 = p^1$$
$$p'^2 = p^2 \tag{3.35}$$
$$p'^3 = -\gamma\beta p^0 + \gamma p^3.$$

---

[3]In particle physics, mostly Lorentz boost in z direction is taken.
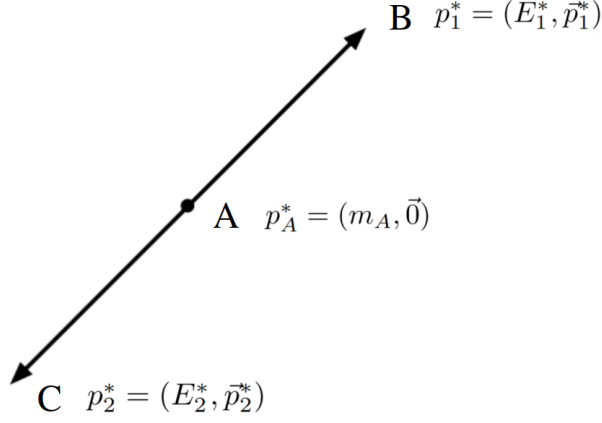
Figure 3.2: Two body decay in the rest frame of the parent particle [12].

From Eqn. 3.32 $p^{\mu} = (E, p_x, p_y, p_z)$ then,

$$\begin{aligned}
E &= \gamma E - \gamma \beta p_z \\
p'_x &= p_x \\
p'_y &= p_y \\
p'_z &= -\gamma \beta E + \gamma p_y
\end{aligned} \tag{3.36}$$

3.2 Kinematics of charged pion decay to muon and neutrino

The neutrino beam in T2K experiment is produced from the 2–body decay of charged $\pi^{\pm}$ into (anti–)neutrinos. The decay processes of π^+ and π^- are:

$$\begin{aligned}
\pi^+ &\longrightarrow \mu^+ + \nu_{\mu} \\
\pi^- &\longrightarrow \mu^- + \overline{\nu}_{\mu}
\end{aligned} \tag{3.37}$$

T2K experiment uses the off–axis beam technique to ensure that the neutrino flux peaks around the energy that corresponds to the oscillation maximum (i.e 0.6 GeV). To understand the kinematics of the off–axis beam we need to understand the kinematics of 2–body decay of $\pi^{\pm}$ in flight. For the ease of calculation, the energy and angle of the daughter particles are calculated in the rest frame of the parent pion (CM frame) first and then transformed into the frame of the pion in flight (lab frame) using Lorentz transformations.

3.2.1 Decay of a particle to two daughter particles

Consider the decay of a parent particle A (of mass m) into two daughter particles B and C (of mass m_1 and m_2 respectively), in the rest frame of A (CM frame) [59] [60]as shown in Fig. 3.2.

$$A \longrightarrow B + C \tag{3.38}$$

The coordinates in the CM frame are denoted by * (starred components).

$$p_A^{*\mu} = (E_A^*, p_A^{*x}, p_A^{*y}, p_A^{*z}), \tag{3.39}$$

33

$$p_A^{*\,2} = (E_A^*)^2 - (\vec{p_A^*})^2 = m_A^2$$
$$p_1^{*2} = (E_1^*)^2 - (\vec{p_1^*})^2 = m_1^2 \qquad (3.40)$$
$$p_2^{*2} = (E_2^*)^2 - (\vec{p_2^*})^2 = m_2^2$$

for daughter particles of well defined masses and $c = 1$ in natural units. Since A is at rest, by the conservation of 3–momentum,

$$\vec{p_A^*} = \vec{p_1^*} + \vec{p_2^*} = 0; \qquad (3.41)$$

therefore,

$$\vec{p_1^*} = -\vec{p_2^*}. \qquad (3.42)$$

i.e, the daughter particles are emitted back to back in the parent's rest frame.

In the rest frame of A, the 4–momentum components of A, B and C are:

$$p_A^* = (m_A, \vec{0})$$
$$p_1^* = (E_1^*, \vec{p_1^*}) \qquad (3.43)$$
$$p_2^* = (E_2^*, \vec{p_2^*})$$

respectively. The daughter particles are defined by 8 components - 2 energies and 6 momenta. Let the 4–momentum equation of the process in Fig. 3.2 be:

$$p_A^* = p_1^* + p_2^* \qquad (3.44)$$

We are now going to find the energy and momentum of particle B with 4–momentum p_1^*. From the 4–momentum equation 3.44:

$$p_2^* = p_A^* - p_1^*. \qquad (3.45)$$

Squaring p_2^2,

$$p_2^{*2} = (p_A^* - p_1^*)^2 = p_A^{*\,2} - 2p_A^*.p_1^* + p_1^{*2}. \qquad (3.46)$$

Since

$$p^2 = E^2 - \vec{p}^{\,2} = m^2,$$

substituting the components of 4–momenta from Eqn. 3.43,

$$p_2^{*2} = p_A^{*\,2} - 2p_A^*.p_1^* + p_1^{*2}$$
$$= m_A^2 - 2p_A^*.p_1^* + p_1^{*2}$$
$$= m_A^2 - 2m_A E_1^* + m_1^2$$
$$= m_2^2.$$

i.e,

$$m_2^2 = m_A^2 - 2m_A E_1^* + m_1^2 \qquad (3.47)$$

Then the energy E_1^* of particle B in the CM frame can be calculated in terms of the masses of the parent and daughter particles as:

$$E_1^* = \frac{m_A^2 + m_1^2 - m_2^2}{2m_A}. \qquad (3.48)$$

Similarly the energy E_2^* of particle C in the CM frame is

$$E_2^* = \frac{m_A^2 + m_2^2 - m_1^2}{2m_A} \tag{3.49}$$

Momenta of particles B and C are :

$$
\begin{aligned}
p_1^* &= [E_1^{*2} - m_1^2]^{1/2} \\
p_2^* &= [E_2^{*2} - m_2^2]^{1/2}
\end{aligned}
\tag{3.50}
$$

respectively. These equations can be used to find the energy and momentum of muons and neutrino produced when charged pions decay.

Energy of neutrino produced from a pion decaying in flight

In actuality, the charged pion, boosted in the z–direction decays in flight, into a neutrino and muon. Here we need to calculate the energy of the neutrino in the lab frame as a function of the parent pion energy and the angle which it makes with the pion direction. The energy of the neutrino in the CM frame is found first using the method discussed in section. 3.2.1. Denoting the 4–momenta components of π^+, μ^+ and ν_μ in the CM frame by Eqn. 3.51,

$$
\begin{aligned}
p_{\pi^+}^* &= (m_{\pi^+}, 0) \\
p_{\nu_\mu}^* &= (E_{\nu_\mu}^*, \vec{p_{\nu_\mu}^*}) \\
p_\mu^* &= (E_\mu^*, \vec{p_\mu^*}),
\end{aligned}
\tag{3.51}
$$

energy of ν_μ in the pion rest frame is

$$E_\nu^* = \frac{m_{\pi^+}^2 + m_\nu^2 - m_\mu^2}{2m_\pi}. \tag{3.52}$$

The mass of neutrino is almost zero, so setting $m_\nu \approx 0$ in Eqn. 3.52, energy of the neutrino in the CM frame is :

$$E_\nu^* = \frac{m_{\pi^+}^2 - m_\mu^2}{2m_\pi}. \tag{3.53}$$

Substituting the values of the masses of π^+ and μ^+ in Eqn. 3.53 we get a constant value for the neutrino energy in the CM frame. With

$$m_{\pi^+} = 139.6 \text{MeV/c}^2; m_\mu = 105.7 \text{MeV/c}^2, \tag{3.54}$$

($c = 1$ in natural units) neutrino energy $E_\nu^* = 29.78$ MeV.

3.2.2   Pion decay in flight

Now consider the decay of π^+ in flight. Here the π^+ is boosted along the z direction with a velocity v. Then the energies of and the angles made by the daughter ν_μ and μ^+ will be different from those in the rest frame of π^+.
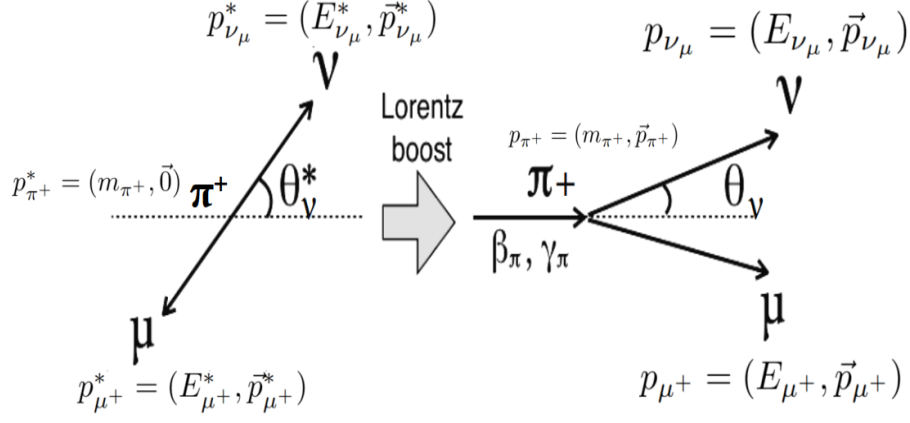
Figure 3.3: Two–body decay of pion in the rest frame of the pion and in flight.

The components of 4–momenta of the particles in the lab frame are:

$$p_{\pi^+} = (m_{\pi^+}, \vec{p}_{\pi^+})$$
$$p_{\nu_\mu} = p_\nu = (E_{\nu_\mu}, \vec{p}_{\nu_\mu}) = (E_\nu, \vec{p}_\nu) \tag{3.55}$$
$$p_{\mu^+} = p_\mu = (E_{\mu^+}, \vec{p}_{\mu^+}) = (E_\mu, \vec{p}_\mu),$$

In the lab frame, by 4–momentum conservation,

$$p_{\pi^+} = p_\mu + p_\nu. \tag{3.56}$$

The 4–momenta components of the daughter μ^+ and ν_μ in the CM frame can be written in spherical polar coordinates as shown in Eqn. 3.57 and 3.58 respectively :

$$p_{\mu^+}^* = (p_{\mu^+}^{0*}, \vec{p}_{\mu^+}^{\,*}) = (p_{\mu^+}^{0*}, p_{\mu^+}^{x*}, p_{\mu^+}^{y*}, p_{\mu^+}^{z*})$$
$$p_{\mu^+}^{x*} = |\vec{p}_{\mu^+}^{\,*}| sin\theta_{\mu^+}^*$$
$$p_{\mu^+}^{y*} = 0 \tag{3.57}$$
$$p_{\mu^+}^{z*} = |\vec{p}_{\mu^+}^{\,*}| cos\theta_{\mu^+}^*,$$

where $|\vec{p}_{\mu^+}^{\,*}| = \sqrt{\Sigma_i (p_{\mu^+}^{i*})^2}$, where $i = x, y, z$.

$$p_\nu^* = (p_\nu^{0*}, \vec{p}_\nu^{\,*}) = (p_\nu^{0*}, p_\nu^{x*}, p_\nu^{y*}, p_\nu^{z*})$$
$$p_\nu^{x*} = |\vec{p}_\nu^{\,*}| sin\theta_\nu^*$$
$$p_\nu^{y*} = 0 \tag{3.58}$$
$$p_\nu^{z*} = |\vec{p}_\nu^{\,*}| cos\theta_\nu^*,$$

where $|\vec{p}_\nu^*| = \sqrt{\Sigma_i (p_\nu^{i*})^2}$, where $i = x, y, z$.

Since in the CM frame μ^+ and ν_μ are emitted back to back, their 3–momenta are equal but opposite. i.e,

$$\vec{p}_\nu^{\,*} = -\vec{p}_{\mu^+}^{\,*}. \tag{3.59}$$

However, we are interested in the kinematics of ν_μ, so from here on we will concentrate on the energy and direction of ν_μ in the CM and lab frames. In the lab frame,

36

the 4–momenta components of ν_μ can be written as in Eqn. 3.60:

$$
\begin{aligned}
p_\nu &= (p_\nu^0, \vec{p}_\nu) = (p_\nu^0, p_\nu^x, p_\nu^y, p_\nu^z) \\
p_\nu^x &= |\vec{p}_\nu| \sin \theta_\nu \\
p_\nu^y &= 0 \\
p_\nu^z &= |\vec{p}_\nu| \cos \theta_\nu,
\end{aligned}
\tag{3.60}
$$

where $|\vec{p}_\nu| = \sqrt{\Sigma_i (p_\nu^i)^2}$, where $i = x, y, z$.

To obtain the energy and direction of ν_μ in the lab frame, apply Lorentz transformations of the 4–momenta components:

$$
p_\nu = \Lambda p_\nu^*,
\tag{3.61}
$$

where

$$
\Lambda = \begin{pmatrix}
\gamma & 0 & 0 & \gamma\beta \\
0 & 1 & 0 & 0 \\
0 & 0 & 1 & 0 \\
\gamma\beta & 0 & 0 & \gamma
\end{pmatrix}
\tag{3.62}
$$

$$
p_\nu = \begin{pmatrix}
\gamma & 0 & 0 & \gamma\beta \\
0 & 1 & 0 & 0 \\
0 & 0 & 1 & 0 \\
\gamma\beta & 0 & 0 & \gamma
\end{pmatrix}
\begin{pmatrix}
p_\nu^{0*} \\
|\vec{p}_\nu^*| \sin \theta_\nu^* \\
0 \\
|\vec{p}_\nu^*| \cos \theta_\nu^*
\end{pmatrix}
=
\begin{pmatrix}
p_\nu^{0*}(\gamma + \gamma\beta \cos \theta_\nu^*) \\
|\vec{p}_\nu^*| sin\theta_\nu^* \\
0 \\
|\vec{p}_\nu^*|(\gamma\beta + \gamma \cos \theta_\nu^*)
\end{pmatrix}
\tag{3.63}
$$

where,

$$
\beta = \frac{\vec{p}_{\pi^+}}{E_{\pi^+}}; \quad \gamma = \frac{E_{\pi^+}}{m_{\pi^+}},
\tag{3.64}
$$

E_{π^+} and $\vec{p}_{\pi^+}$ are the energy and 3–momenta of π^+ in the lab frame and m_{π^+} is the rest π^+.

By relativistic energy–momentum relation ,

$$
\begin{aligned}
p_\nu^{0*} &= E_\nu^* = |\vec{p}_\nu^*| \text{ and} \\
p_\nu^0 &= E_\nu = |\vec{p}_\nu|,
\end{aligned}
\tag{3.65}
$$

since the mass of the neutrino $m_\nu \approx 0$. Thus from Eqns. 3.63 and 3.65 we get,

$$
p_\nu^0 = E_\nu = \gamma E_\nu^* (1 + \beta \cos \theta_\nu^*)
\tag{3.66}
$$

and

$$
p_\nu^z = E_\nu \cos \theta_\nu = \gamma E_\nu^* (\cos \theta_\nu^* + \beta)
\tag{3.67}
$$

where, β and γ are given in Eqn. 3.64.

From Eqns. 3.60 and 3.65, the components of p_ν, the 4–momentum in the lab frame can be written as:

$$p_\nu = (p_\nu^0, p_\nu^1, p_\nu^2, p_\nu^3) = (E_\nu, E_\nu \sin\theta_\nu, 0, E_\nu \cos\theta_\nu). \tag{3.68}$$

From Eqns. 3.66 and 3.67,

$$\cos\theta_\nu = \frac{p_\nu^0}{p_\nu^z} = \frac{\gamma E_\nu^* [cos\theta_\nu^* + \beta]}{\gamma E_\nu^* [1 + \beta \cos\theta_\nu^*]} = \frac{[\beta + \cos\theta_\nu^*]}{[1 + \beta \cos\theta_\nu^*]}. \tag{3.69}$$

Multiplying Eqn. 3.69 with β, and subtracting from 1,

$$1 - \beta cos\theta_\nu = \frac{(1 - \beta^2)}{(1 + \beta cos\theta_\nu^*)} \tag{3.70}$$

Rearranging,

$$(1 - \beta \cos\theta_\nu)(1 + \beta \cos\theta_\nu^*)\gamma^2 = 1 \tag{3.71}$$

since

$$\gamma = \frac{1}{\sqrt{1 - \beta^2}} \tag{3.72}$$

$$\gamma^2 = \frac{1}{1 - \beta^2}. \tag{3.73}$$

When $\theta_\nu^* = 0$; $\cos\theta_\nu^* = 1$. Then from Eqns. 3.70 and 3.71,

$$\cos\theta_\nu = \frac{1 + \beta}{1 + \beta} = 1. \tag{3.74}$$

Since $cos\theta_\nu = 1$, $\theta_\nu = 0$.

When $\theta_\nu^* = \dfrac{\pi}{2}$, $\cos\theta_\nu^* = 0$. Then from Eqn. 3.71,

$$\cos\theta_\nu = \frac{\gamma^2 - 1}{\beta\gamma^2} = \beta = \left(1 - \frac{1}{\gamma^2}\right)^{1/2} \tag{3.75}$$

Then,

$$\cos\theta_\nu^{max} = \beta = \left(1 - \frac{1}{\gamma^2}\right)^{1/2}. \tag{3.76}$$

From Eqn. 3.66, energy of the neutrino in the lab frame is given by

$$E_\nu = \gamma E_\nu^* \left(1 + \beta \cos\theta_\nu^*\right),$$

where γ and β are defined in Eqn. 3.64, E_ν^* is the neutrino energy in the CM frame given by Eqn. 3.51, θ_ν is the angle the neutrino makes with the direction of π^+ in the lab frame and θ_ν^* is the neutrino angle in the CM frame. Substituting the expressions from Eqn. 3.64, 3.51 and 3.71, E_ν in the lab frame can be expressed as:

$$E_\nu = \left(\frac{E_{\pi^+}}{m_{\pi^+}}\right)\left(\frac{m_{\pi^+} - m_\mu}{2m_{\pi^+}}\right)\left[\frac{1}{\gamma^2(1 - \beta \cos\theta_\nu)}\right]. \tag{3.77}$$

For small θ_ν, the Taylor series expansion of $\cos\theta_\nu$ is:

$$cos\theta_\nu = 1 - \frac{\theta_\nu^2}{2!} + \frac{\theta_\nu^4}{4!} - ...$$

Neglecting the higher order terms,

$$\cos\theta_\nu = 1 - \frac{\theta_\nu^2}{2}. \tag{3.78}$$

Substituting the value of $\cos\theta_\nu$ from Eqn.3.78 into Eqn. 3.77 gives

$$E_\nu = \frac{\gamma E_\nu^*}{\gamma^2 \left[1 - \beta\left(1 - \frac{\theta_\nu^2}{2}\right)\right]} \tag{3.79}$$

Multiplying the numerator and denominator of Eqn. 3.79 by $(1+\beta)$ and simplifying by making use of Eqn. 3.73, we get

$$E_\nu = \frac{\gamma E_\nu^*(1+\beta)}{\left[1 + \left(\frac{\gamma^2 \beta \theta_\nu^2(1+\beta)}{2}\right)\right]} \tag{3.80}$$

The π^+ has very high energy (ultra–relativistic), so we can take $\beta \approx 1$. Then Eqn.3.80 becomes

$$E_\nu = \frac{2\gamma E_\nu^*}{1 + \gamma^2 \theta_\nu^2}. \tag{3.81}$$

We want the neutrino energy in lab frame as a function of pion energy E_{π^+} and θ_ν, the angle which the neutrino makes with the pion direction. Substituting the expressions for γ from Eqn. 3.64 and E_ν^* from Eqn. 3.53 and simplifying, we get

$$E_\nu = \left(1 - \frac{m_\mu^2}{m_{\pi^+}^2}\right) \frac{E_{\pi^+} m_{\pi^+}^2}{\left[m_{\pi^+}^2 + E_{\pi^+}^2 \theta_\nu^2\right]}. \tag{3.82}$$

Substituting the values of m_{π^+} and m_μ from Eqn. 3.54, we get

$$E_\nu = 0.43 \left(\frac{E_{\pi^+} m_{\pi^+}^2}{m_{\pi^+}^2 + E_{\pi^+}^2 \theta_\nu^2}\right). \tag{3.83}$$

When $\theta_\nu = 0°$, ν_μ is *on–axis* compared to π^+ direction (i.e in the same direction as π^+) and there is a linear relation between E_ν and E_{π^+}:

$$E_\nu = 0.43 E_{\pi^+}. \tag{3.84}$$

This can lead to a wide band (WB) neutrino beam if the range of E_{π^+} is wide.

When $\theta_\nu > 0°$, ν_μ is *off–axis*, i.e ν_μ is emitted in a direction different from the direction of π^+. Since, both the numerator and denominator of Eqn. 3.83 increase with E_{π^+}, there is a quenched dependence of E_ν on E_{π^+}. Taking the derivative of E_ν w.r.to E_{π^+} illustrates this quantitatively:

$$\frac{dE_\nu}{dE_{\pi^+}} = \left(1 - \frac{m_\mu^2}{m_{\pi^+}^2}\right) \frac{(1 - \gamma^2 \theta_\nu^2)}{(1 + \gamma^2 \theta_\nu^2)^2}. \tag{3.85}$$

The derivative becomes 0 when $\theta_\nu = \gamma^{-1} = \dfrac{m_{\pi^+}}{E_{\pi^+}}$ and

$$E_\nu \simeq \left(1 - \frac{m_\mu^2}{m_{\pi^+}^2}\right)\frac{m_{\pi^+}}{2\theta_\nu} \simeq \frac{29.79\text{MeV}}{\theta_\nu}. \qquad (3.86)$$

For an average pion energy $\langle E_{\pi^+}\rangle$, a detector kept at an off–axis angle of $\theta_\nu = \dfrac{m_{\pi^+}}{\langle E_{\pi^+}\rangle}$ receives neutrino beam which is almost monochromatic. The average energy of this near monochromatic beam is given by Eqn. 3.86.

The dependence of E_ν on E_{π^+} and θ_ν is illustrated in Fig. 3.4.
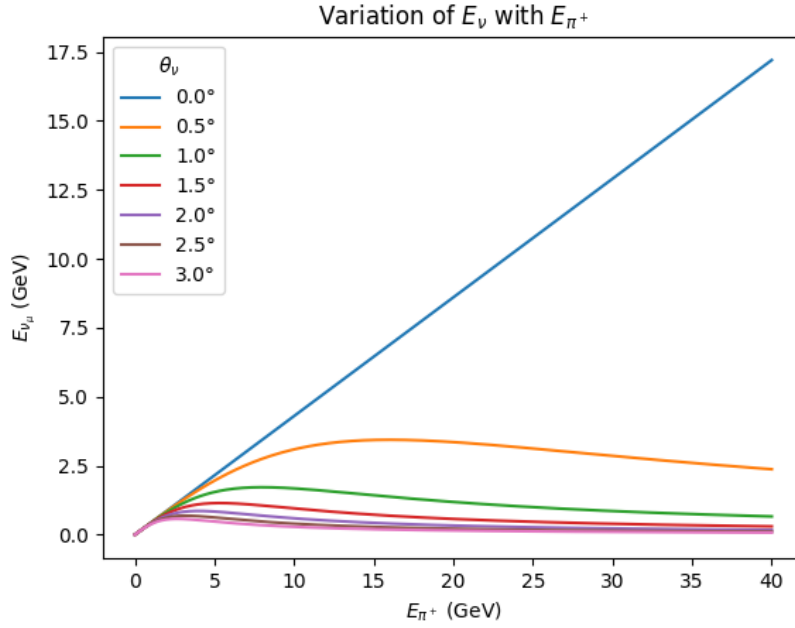
Figure 3.4: Variation of neutrino energy E_ν with the energy of the parent π^+, E_{π^+} and neutrino angle θ_ν in the lab frame.

The on–axis configuration corresponds to $\theta_\nu = 0°$ (blue line) where E_ν and E_{π^+} have a linear relation. Off–axis, E_ν is almost constant in the range of E_{π^+} shown in Fig. 3.4. Also $E_\nu < E_{\pi^+}$, which leads to a shorter oscillation length and enhances the sensitivity to small mass squared differences in neutrino oscillations. A neutrino energy $E_\nu = 0.6$ GeV is obtained at $\theta_\nu = 2.5°$. This is the reason why T2K experiment, which has a baseline of 295 km, whose oscillation maxima occurs at 0.6 GeV, has the near and far detectors at an off–axis angle of 2.5°.

3.2.3 Variation of relative flux with neutrino energy

In a neutrino experiment it is important to estimate the flux of neutrinos, since the number of detected neutrino events also depends on the flux. In this section, an analytical expression for the energy–angle spectrum $\dfrac{d^2N}{dE_\nu d\Omega_\nu}$ in terms of the quantities E_ν, θ_ν and ϕ_ν (in the lab frame) will be derived [61]. Here, $d\Omega$ is the solid angle and by definition

$$d\Omega_\nu \propto d\cos\theta_\nu. \qquad (3.87)$$

The energy–angle spectrum is uniform in the azimuthal angle ϕ_ν and is flat in $\cos\theta_\nu^*$ in the rest frame of π^+.

The parent pions are produced with an energy spectrum

$$\frac{dN}{dE_{\pi^+}} \propto (E_p - E_{\pi^+})^5, \tag{3.88}$$

where, E_p is the energy of the proton beam and E_{π^+} is the energy of the π^+ beam. The energy angle spectrum calculation requires the following transformation:

$$\frac{d^2N}{dE_\nu d\Omega_\nu} \propto \frac{d^2N}{dE_\nu d\cos\theta_\nu} = \frac{d^2N}{dE_{\pi^+}d\cos\theta_\nu^*} J(E_{\pi^+}, \cos\theta_\nu^*, E_\nu, \cos\theta_\nu)$$
$$\propto (E_p - E_{\pi^+})^5 J \tag{3.89}$$

$$\frac{d^2N}{dE_\pi d\cos\theta_\nu^*} \propto (E_p - E_\pi)^5 \tag{3.90}$$

The Jacobian is given by :

$$J(E_{\pi^+}, \cos\theta_\nu^*, E_\nu, \cos\theta_\nu) = \begin{vmatrix} \dfrac{\partial E_{\pi^+}}{\partial E_\nu} & \dfrac{\partial\cos\theta_\nu^*}{\partial E_\nu} \\[2mm] \dfrac{\partial E_{\pi^+}}{\partial\cos\theta_\nu} & \dfrac{\partial\cos\theta_\nu^*}{\partial\cos\theta_\nu} \end{vmatrix} \tag{3.91}$$

Since the exact form of this Jacobian is lengthy it is simplified to some extent by noting that for a high energy neutrino beam with $E_\nu \gg m_{\pi^+}$, the parent π^+ is also ultra–relativistic and hence $\beta \approx 1$, where β is given by Eqn. 3.64. The θ_ν is very small for any value of θ_ν^*, for ultra–relativistic particles. The relation between θ_ν and θ_ν^* is obtained from Eqns. 3.58, 3.60, 3.67 and 3.66 assuming $\beta \approx 1$ (ultra–relativistic case).

$$\tan\theta_\nu = \frac{E_\nu^*}{E_\nu}\sin\theta_\nu^*$$
$$\therefore\ \sin\theta_\nu^* = \frac{E_\nu}{E_\nu^*}\tan\theta_\nu \tag{3.92}$$

From Eqn. 3.92,

$$\cos\theta_\nu^* = \sqrt{1 - \sin^2\theta_\nu^*} = \sqrt{1 - \frac{E_\nu^2\tan^2\theta_\nu}{E_\nu^{*2}}} = \sqrt{1 - \frac{E_\nu^2}{E_\nu^{*2}}\left(\frac{1}{\cos^2\theta_\nu^*} - 1\right)}. \tag{3.93}$$

Hence

$$\frac{\partial\cos\theta_\nu^*}{\partial E_\nu} = \frac{\partial}{\partial E_\nu}\sqrt{1 - \frac{E_\nu^2\tan^2\theta_\nu}{E_\nu^{*2}}}$$
$$= -\frac{E_\nu\tan^2\theta_\nu}{E_\nu^*(E_\nu^{*2} - E_\nu^2\tan^2\theta_\nu)^{1/2}} = -\frac{E_\nu}{E_\nu^{*2}}\frac{\tan^2\theta_\nu}{\cos\theta_\nu^*}, \tag{3.94}$$

using Eqn. 3.92. For $\theta_\nu \longrightarrow 0°$, $\sin\theta_\nu \longrightarrow \theta_\nu \implies \tan^2\theta_\nu \longrightarrow \theta_\nu^2$.

Then Eqn. 3.94 becomes

$$\frac{\partial\cos\theta_\nu^*}{\partial E_\nu} = \frac{-E_\nu\theta_\nu^2}{E_\nu^{*2}\cos\theta_\nu^*} \tag{3.95}$$

The partial derivative

$$\frac{\partial \cos \theta_\nu^*}{\partial \cos \theta_\nu} = \frac{\partial}{\partial \cos \theta_\nu} \sqrt{1 - \frac{E_\nu^2}{E_\nu^{*2}} \left(\frac{1}{\cos^2 \theta_\nu^*} - 1 \right)}$$

$$= \frac{E_\nu^2}{E_\nu^{*2} \cos^3 \theta_\nu} \frac{1}{\sqrt{\left[1 - \frac{E_\nu^2 \tan^2 \theta_\nu}{E_\nu^{*2}} \right]}} = \frac{E_\nu^2}{E_\nu^{*2} \cos^3 \theta_\nu \cos \theta_\nu^*}, \tag{3.96}$$

using Eqn. 3.92.

When $\theta_\nu \longrightarrow 0°$, $\cos \theta_\nu \longrightarrow 1 \implies \cos^3 \theta_\nu \longrightarrow 1$. Then Eqn. 3.96 simplifies to

$$\frac{\partial \cos \theta_\nu^*}{\partial \cos \theta_\nu} = \frac{E_\nu^2}{E_\nu^{*2} \cos \theta_\nu^*}. \tag{3.97}$$

From the component notation of the 4–momenta in Eqn.3.68 and 3.63,

$$p_\nu = (E_\nu, \ E_\nu \sin \theta_\nu, \ 0, \ E_\nu \cos \theta_\nu)$$
$$= (\gamma E_\nu^* [1 + \beta \cos \theta_\nu^*], \ E_\nu^* \sin \theta_\nu^*, \ 0, \ \gamma E_\nu^* [\beta + \cos \theta_\nu^*]) \tag{3.98}$$

where γ and β are defined in Eqn. 3.64.

Equating the time components in Eqn. 3.98,

$$E_\nu = \gamma E_\nu^* \left(1 + \beta \cos \theta_\nu^* \right). \tag{3.99}$$

For ultra–relativistic π^+, $\beta \approx 1$. Then from Eqn. 3.99,

$$\gamma = \frac{E_{\pi^+}}{m_{\pi^+}} = \frac{E_\nu}{E_\nu^* (1 + \cos \theta_\nu^*)} \tag{3.100}$$

and

$$E_{\pi^+} = \frac{E_\nu m_{\pi^+}}{E_\nu^* (1 + \cos \theta_\nu^*)}. \tag{3.101}$$

Taking the partial derivative of E_{π^+} in Eqn. 3.101 w.r.to E_ν,

$$\frac{\partial E_{\pi^+}}{\partial E_\nu} = \frac{m_{\pi^+}}{E_\nu^* (1 + \cos \theta_\nu^*)} - \frac{m_{\pi^+} E_\nu}{E_\nu^* (1 + \cos \theta_\nu^*)^2} \left(\frac{\partial \cos \theta_\nu^*}{\partial E_\nu} \right). \tag{3.102}$$

Using Eqns. 3.66 and 3.94,

$$\frac{\partial E_{\pi^+}}{\partial E_\nu} = \frac{E_{\pi^+}}{E_\nu} + \frac{E_{\pi^+}^2 \theta_\nu^2}{m_{\pi^+} E_\nu^* \cos \theta_\nu^*}. \tag{3.103}$$

The remaining term in the Jacobian can be found as,

$$\frac{\partial E_{\pi^+}}{\partial \cos \theta_\nu} = \frac{\partial}{\partial \cos \theta_\nu} \left[\frac{m_{\pi^+} E_\nu}{E_\nu^* (1 + \cos \theta_\nu^*)} \right] = -\frac{m_{\pi^+} E_\nu}{E_\nu^* (1 + \cos \theta_\nu^*)^2} \left(\frac{\partial \cos \theta_\nu^*}{\partial \cos \theta_\nu} \right) \tag{3.104}$$

Substituting the values of $\left(\frac{\partial \cos \theta_\nu^*}{\partial \cos \theta_\nu} \right)$ and γ from Eqns. 3.97 and 3.64 and simplifying, Eqn. 3.104 becomes

$$\frac{\partial E_{\pi^+}}{\partial \cos\theta_\nu} = -\frac{E_\nu E_\pi^2}{m_{\pi^+} E_\nu^* \cos\theta_\nu^*} \tag{3.105}$$

Substituting Eqns. 3.95 , 3.97 , 3.103 and 3.105 in Eqn. 3.91 gives the Jacobian as

$$J = \begin{vmatrix} \dfrac{E_{\pi^+}}{E_\nu} + \dfrac{E_{\pi^+}^2 \theta_\nu^2}{m_{\pi^+} E_\nu^* \cos\theta_\nu^*} & -\dfrac{E_\nu \theta_\nu^2}{E_\nu^{*2} \cos\theta_\nu^*} \\ -\dfrac{E_\nu E_{\pi^+}^2}{m_{\pi^+} E_\nu^* \cos\theta_\nu^*} & \dfrac{E_\nu^2}{E_\nu^{*2} \cos\theta_\nu^*} \end{vmatrix} \tag{3.106}$$

Taking the determinant gives

$$J(E_{\pi^+}, \cos\theta_\nu^*, E_\nu, \cos\theta_\nu) = \frac{E_{\pi^+} E_\nu}{E_\nu^* \cos\theta_\nu^*}. \tag{3.107}$$

Hence the energy–angle spectrum from Eqn. 3.88 can be written as

$$\frac{d^2 N}{dE_\nu d\cos\theta_\nu} \propto (E_p - E_{\pi^+})^5 \frac{E_{\pi^+} E_\nu}{E_\nu^* \cos\theta_\nu^*} \tag{3.108}$$

Since the $p_\mu^* = p_\nu^*$, the energy-angle spectrum for neutrino and muons will be identical. Since the factor in the denominator $\cos\theta_\nu^*$ can go to zero, ν_μ flux may be higher for non–zero lab angle θ_ν i.e, for an off–axis case. Note that in this chapter the calculations were shown for the 2–body decay of π^+ which produces ν_μ beam. The calculation of kinematics for the 2–body decay of π^- which produces the anti–neutrino beam $\bar\nu_\mu$ is identical.

CHAPTER 4

Photo Multiplier Tubes (PMTs)

Photo multiplier tubes (PMTs) are electron device tubes that convert light to an electric current. These are very sensitive devices and are indispensable in many neutrino experiments [53] [55] [62] [63] [64]. Other fields of high energy physics, nuclear physics, spectroscopy and biotechnology also employ PMTs today[65][66]. A discussion of the basic properties of PMTs and their responses to the variations in properties and parameters is presented in this chapter.

4.1 Photo Electric Effect

The first step of PMT operation is the production of photo electrons when a photocathode detects light. PMTs have a layer of photocathode on which the photons are incident and produce photo electrons. The process which enables this is the photoelectric effect which was discovered by Henrich Hertz[67] in 1887, and was confirmed in 1888 by Hallwachs[68]. In 1889, Elster and Geitel[69] reported that the photoelectric effect was induced not only by UV radiation but also by visible light incident on an alkali metal like sodium or potassium. The theory of photoelectric effect was given by Einstein[70] in the year 1905 for which he was awarded the Physics Nobel in 1921 [71]. By Einstein's photoelectric equation [13], [72]:

$$E = h\nu - \phi, \tag{4.1}$$

where E is the kinetic energy of the emitted electron, h is Planck's constant 6.626×10^{-34} Js and ν is frequency of the incident light (in Hz). The work function ϕ of the material is

$$\phi = h\nu_0 \tag{4.2}$$

where the ν_0 is the minimum frequency required for the photoelectric effect to occur [72].

4.2 Basics of PMTs

A photo multiplier tube is a glass vacuum tube [13] with the following parts :

- an input glass window through which light enters the PMT
- a *photocathode*, whose electrons are excited and emitted if the light has sufficient frequency
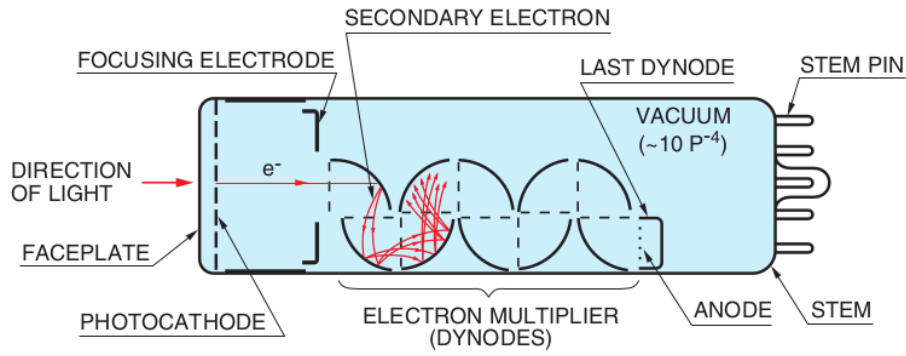
44

Figure 4.1: Schematic of a photo multiplier tube [13].

– focusing electrodes which accelerate the photo electrons and focus them to the first electron multiplier

– electron multipliers known as *dynodes* where secondary electrons are emitted when the photo electrons hit them

– an *anode* where a cluster of amplified secondary electrons is extracted from.

The secondary electrons multiply at each dynode resulting in a cluster amplified upto $10^6 - 10^7$ times by the last dynode stage.

The schematic of a PMT is shown in Fig. 4.1.

A potential "ladder" is set up by applying a high potential to the cathode, dynodes and the anode. The following processes occur in a PMT:

– A photo electron is emitted via photo electric effect when a photon impinges the photocathode.

– Because of the applied voltage, the photo electron is focussed and accelerated towards the first dynode.

– The photo electron incident on the first dynode transfers part of its energy to this dynode, resulting in secondary electron emission.

– These secondary electrons are accelerated and focused to the next dynode and so on till the last dynode. A cascade of secondary electrons are thus released, which results in an amplified electric signal.

– These secondary electrons are collected at the anode and we get an electric current.

4.2.1 Photocathode

A photocathode is a material which emits electrons by absorbing photons. In vacuum glass PMTs, it is a thin layer made of a photoemissive material deposited on the inner surface of the glass window. Photocathodes are usually made of alkali antimonides [73] like SbKCs, SbNa2K and SbNa2KCs [74]. The photocathodes are sensitive to the wavelength of the light incident on them. Bialkali (with two alkali) photo cathodes are usually used to detect light in the blue region of visible spectrum, whereas green–extended bialkali (GEBA) photo cathodes are also sensitive to the green region. High temperature bialkali photocathodes like SbNa2K are preferred for long time use at temperatures $> 60°$. Multi–alkali like SbNa2KCs have a better

45

sensitivity than the bialkali photocathodes in the wavelength range 600–850 nm, but have higher noise. Extended–red multialkali (ERMA) cathodes are thicker with a spectral response extending to 900 nm. GaAs which is sensitive to near infrared and RbCsSb are some other common photocathode materials. Monoalkali photo cathode SbCs3, AgOCs with sensitivity to visible – infrared wavelengths etc are some of the rarely used photocathodes.

Photocathode sensitivity

Quantum efficiency : The sensitivity of a photocathode to light is specified by several methods, the most important of which is the quantum efficiency [72]. Quantum efficiency $\eta(\lambda)$ is the ratio the number of photo electrons emitted from the photocathode to the number of photons incident on it :

$$\eta(\lambda) = \frac{N_{pe}}{N_\gamma(\lambda)}, \tag{4.3}$$

where $N_\gamma(\lambda)$ is the number of photons indicent on the photo cathode, N_{pe} is the number of photo electrons emitted and λ is the wavelength of light incident on the photocathode. Quantum efficiency depends on the photocathode material and the wavelength of the light; $\eta(\lambda) < 0.35$. For each cathode type there is a region of λ with usable values of η. For example the values of $\eta(\lambda)$ vs λ in nm for bialkali photocathodes are shown in Fig. 4.2.
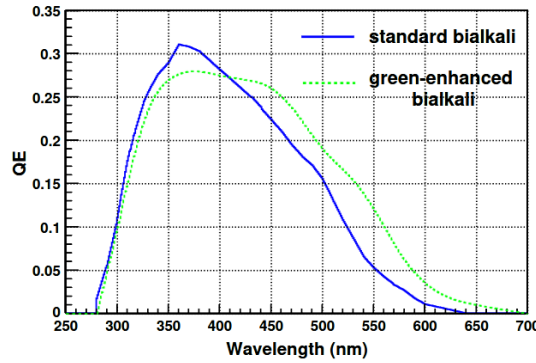
Figure 4.2: Quantum efficiency $\eta\lambda$ vs wavelength of light (λ) in nm for blue–sensitive and green–enhanced bialkali photocathodes. Figure is taken from [14]

Radiant cathode sensitivity While quantum efficiency is defined in terms of the number of photons and photo electrons, it is difficult to count these. But we can measure the current produced at the photocathode corresponding to an incident light power. Radiant cathode sensitivity is defined as

$$E(\lambda) = \frac{I_k}{P(\lambda)} \text{ [Ampere/Watts]}, \tag{4.4}$$

where I_k is photoelectric emission current from the cathode in amperes, $P(\lambda)$ is the incident radiant power in watts and λ is the wavelength in nm. $E(\lambda)$ is related to the quantum efficiency $\eta(\lambda)$ as

$$E(\lambda) = \lambda\eta(\lambda)\frac{e}{hc}, \tag{4.5}$$

where $e = 1.6 \times 10^{-19}$ C is the charge of the electron; $h = 6.626 \times 10^{-34}$ Js is the Planck's constant, $c = 3 \times 10^8$ ms^{-1} is the velocity of light in vacuum and λ is the wavelength in nm. Substituting these values in Eqn. 4.5 and simplifying,

$$E(\lambda) = \frac{\lambda \eta(\lambda)}{1240} \ [A/W] \tag{4.6}$$

4.2.2 Electron optical input system

The electron optical input system collects the photo electrons emitted from the photocathode and focus them to the first dynode. In most PMTs a suitable electric field configuration is applied for collection and focusing of photo electrons. Collection efficiency F is defined as [13]

$$F = \frac{R_{anode}}{R_{pcpe}}, \tag{4.7}$$

where R_{anode} is the count rate at the anode and R_{pcpe} is the rate of photo electron emission from the photocathode.

The electron optical input system must be designed to ensure

- efficient collection of photoelectrons - regardless of the point of their origin on the cathode, as many emitted photo electrons must reach first dynode

- the time taken by the photo electron to travel from the cathode to the first dynode must be as independent to the point of emission.

4.2.3 Electron multiplier system

The weak primary photocurrent from the cathode is amplified using a series of dynodes in the electron multiplier system. Each photo electron hitting a dynode will transfer its kinetic energy to the electrons in the dynode causing secondary electron emission to produce a measurable current at the PMT anode. The gain of each dynode is called the *secondary emission factor* δ.

An electric field is maintained between the dynodes accelerates and focuses the electrons along the multiplier. The secondary emission layer is usually formed by oxidizing or coating the surface of a metal conductor (like beryllium copper Cu–Be) with an alkali antimonide layer [15]. A good dynode should have

- a high average number of seconday electrons emitter per primary electon (i.e high seconday emission factor δ)

- stable secondary emission effect under high currents

- low noise/thermionic emission.

Conventional PMTs have 10–14 dynodes with a total gain upto 10^7. The different dynode configurations in electron multipliers usually used are - linear focusing, venetian–blind, the foil, box or box and grid, circular cage and microchannel plate (MCP). The schematic of these configurations are shown in Fig. 4.3.

Response of the multiplier - single electron spectrum Ideally the gain of the electron–multiplier system should be a constant for all fixed energy electrons entering the dynode system. Due to the statistical nature of the secondary emission process, single electrons of the same energy, entering the system will produce different number of secondary electrons causing flucuations in the multiplier gain. *Single electron spectrum* gives a measure of the extend of the fluctuations in a given multiplier chain from the entry of single electrons only into the multiplier system.

4.2.4 Some PMT operating parameters

Some of the important operating parameters of PMT are the gain and voltage supply. The gain of a PMT depends on the number of dynodes and the secondary emission factor δ which inturn depends on the energy of the primary electron. Since the energy of the electrons incident on each dynode is a function of the inter–dynode potential difference V_d, the secondary emission factor can be written as

$$\delta = KV_d, \tag{4.8}$$

where K is a constant. The gain G of the PMT when the applied voltage is divided equally among all the dynodes is,

$$G = \delta^n = (KV_d)^n, \tag{4.9}$$

where n is the number of dynodes in the PMT [72].

Voltage dividers A single high voltage supply and voltage divider can provide the voltages between the dynodes to accelerate and focus electrons in a PMT. There are three voltage divider circuits used mostly in PMTs, namely *iterative, progressive* and *intermediate progressive* voltage distributions. In iterative voltage distribution, the voltage is the same for all multiplier stages (except the first few). Progressive voltage distribution has increasing voltage from cathode to anode. The intermediate progressive voltage distribution has optimized time characteristics. A schematic of the three different voltage divider configurations are shown in Fig. 4.3.

Before discussing the distribution of anode electrons let us look at the PMTs used in Super–K.

4.2.5 Super–K photo multiplier tubes

SK has 11146, 20 inch (50 cm) PMTs in its inner detector and 1885, 8 inch (20 cm) PMTs in the outer detector. The 50 cm PMTs belong to the Hamamatsu R3600 [75], [51]. These SK PMTS have photocathodes made of bi–alkali materials (Sb–K–Cs) whose quantum efficiencies cut off at the end of the visible spectrum at approximately 650 nm. The photo–cathode is a thin–film on the inner side of the PMT glass bulb. Cherenkov light produced in the target medium in the SK detector is detected with the 20 inch Hamamatsu R3600 PMTs. The ID PMTs collect weak light signals, convert them to photoelectrons and then amplify them so that external circuitry can detect them [76]. The R3600 PMTs have a collection efficiency of 70% and an electron transit time spread of ~ 5.5 ns [75]. To achieve gains of the order of $\sim 10^7$ and a very wide field of view, the 20–inch PMTs have 75 mm $\times$ 75 mm dynodes arranged in a *venetian blind* configuration.
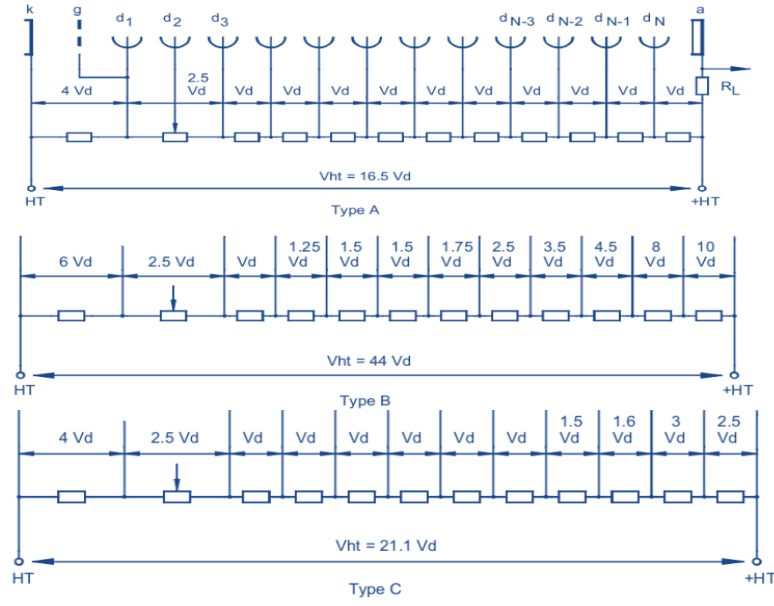
Figure 4.3: Different voltage divider set ups. Type A – iterative, Type B – progressive and Type C – intermediate. V_d is the smallest potential between the dynodes. Figure is taken from [15].

Figure 4.4: A 20 inch diameter Hamamatsu R3600 photo multiplier tube (PMT) in the ID of Super–K [16].

4.3 Distribution of anode electrons

In section. 4.2 we sw several factor affecting the operation and response of PMTs. The main outputs from a PMT are the charge and timing information. The charge depends on the number of electrons collected at the anode. This number inturn depends on the following factors :

- number of photons incident on the photocathode N_γ
- quantum efficiency $\eta(\gamma)$ of the photocathode
- supply voltage V
- inter dynode voltage V_d
- number of dynodes n

The emission of photo electrons as well as secondary electrons are statistical in nature and follow a Poisson distribution [77]. Hence we can model the distribution of the output electrons at the PMT anode using Monte Carlo methods [78]. Photo electron and secondary electron emission can be triggered by the detection of one or more photons [79]. In the following, the anode electron distributions for different combinations of these parameters are studied.

4.3.1 Monte Carlo simulations to generate PMT output

Let N_γ photons of wavelength 400 nm, hit the photocathode of a PMT When photons hit the photocathode photo electrons are emitted. When the photo electrons hit the dynodes with energy E, secondary electron are emitted with an energy directly proportional to the energy of the incoming electrons

$$E_s = \alpha \times E, \qquad (4.10)$$

where the E_s is the energy of the secondary electron and α is a constant. We have to determine the number of photo electrons emitted. Since all photons incident on the photocathode will not cause photo electron emission, the distribution of the emitted photo electrons follows a Poisson distribution [77]. The probability that a photon produces a photo electron is determined by the quantum efficiency $\eta(\gamma)$ of the photocathode. One of the studies performed is with different values of quantum efficiencies to see how it affects the output electron distribution at the anode.

If a photo electron is produced, it will get accelerated towards the first dynode by a potential difference. All the electrons, produced at the photocathode or one of the dynodes are assumed to start with zero kinetic energy. So the energy gained by an electron is $q\Delta V$, where q is the charge of the electron and ΔV is the potential difference between its starting and final positions. In this section the effect of different number of dynodes, supply voltages and inter–dynode potentials are also studied.

The mean number of secondary electrons produced is proportional to the energy of the incoming electron. Again, not all electrons will generate secondary electrons and the secondary electron emission also follows a Poisson distribution [77]. The Monte Carlo (MC) simulations are done for 10^5 iterations. The mean and RMS of the anode electron distribution are also obtained from the distributions.

Values of parameters for MC simulations

Anode electron distributions are plotted for different combinations of the PMT parameters set to the values shown in Table. 4.1.

PMT parameters	Values
Quantum efficiency $(\eta(\lambda))$	0.12, 0.23, 0.33, 0.55
Applied voltage (V)	15 V, 20 V, 25 V
Number of incident photons N_γ	1543, 2363
Dynode potentials	$[0, 50, 100, 150, 200, 250, 300]$
	$[0, 150, 300, 450, 600, 750, 900]$
Number of dynodes n	6,7,8

Table 4.1: PMT parameters and their values used in the Monte Carlo simulation of anode electron distributions. Here 6 and 8 number of dynodes are two special cases. For most of the study the general case is taken as 7 dynodes.

Anode electron distributions - Results

The plots for the anode electron distributions for different cases are given in this section.

Figure 4.5: Distribution of anode electron for dynode potentials [0,150,300,450,600,750,900] for Table. 4.4.

Figure 4.6: Distribution of anode electron for dynode potentials [0,150,300,450,600,750,900] for Table. 4.4.
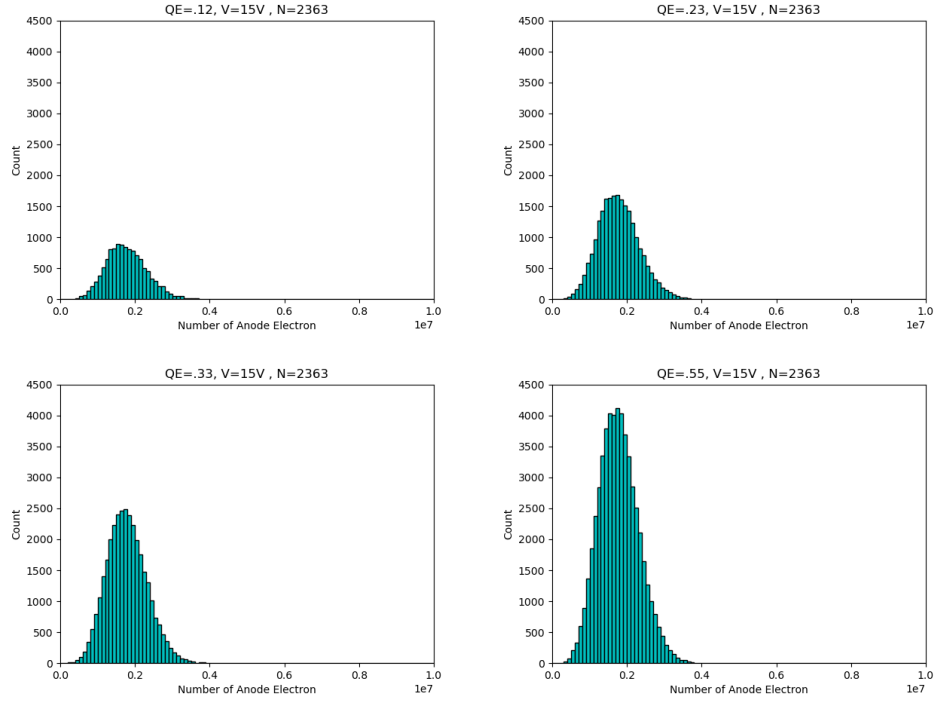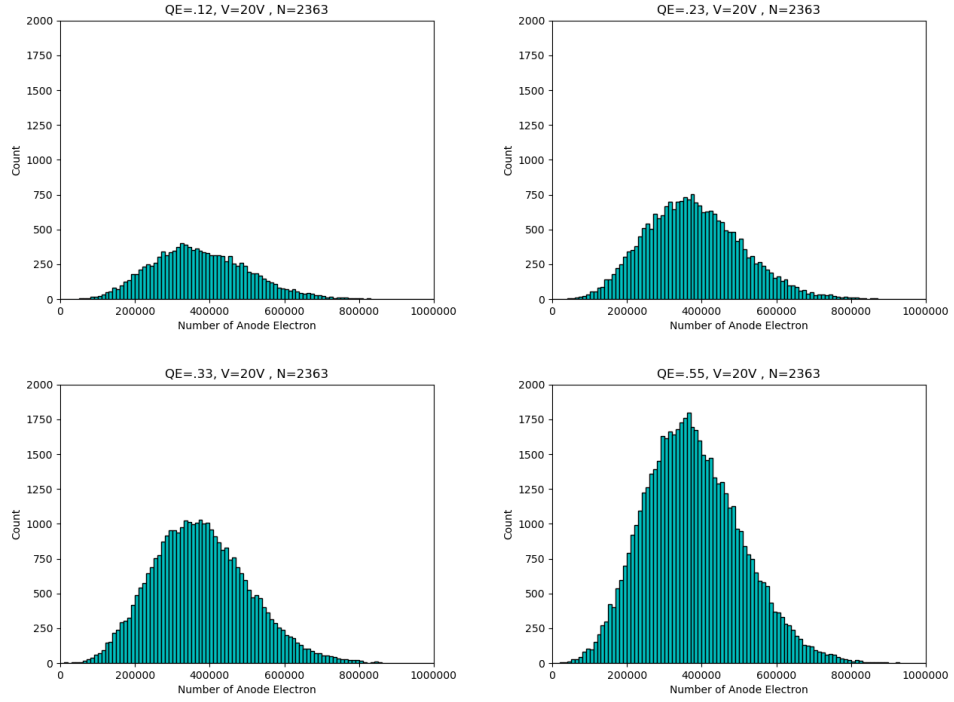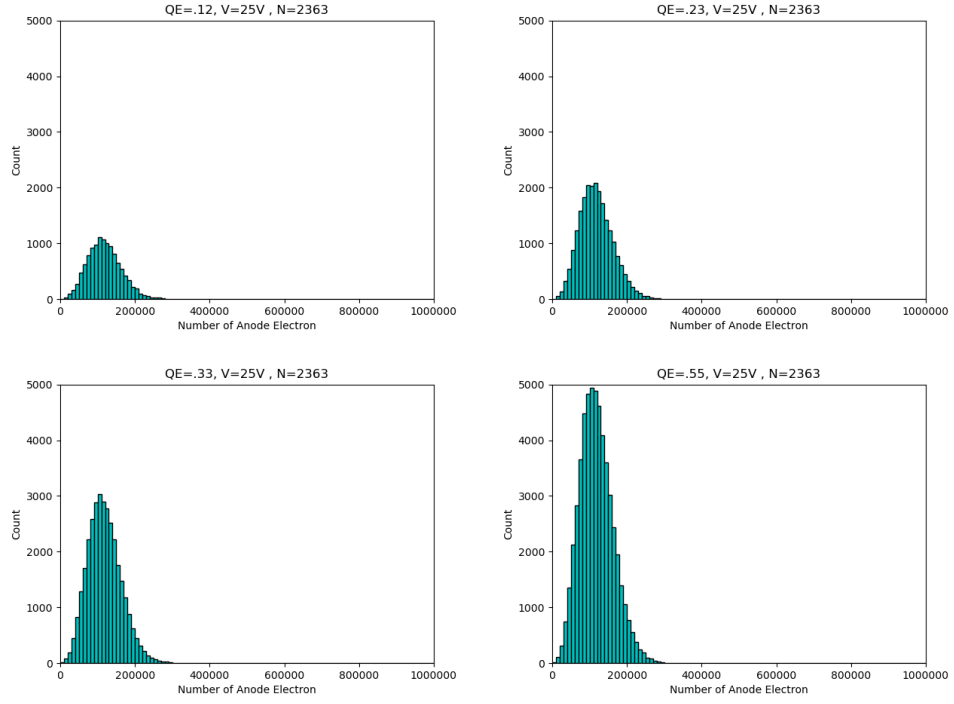
Figure 4.7: Distribution of anode electron for dynode potentials [0,150,300,450,600,750,900] for Table. 4.4.

Figure 4.8: Distribution of anode electrons for dynode potentials: [0,150,300,450,600,750,900] for Table. 4.5.

N_γ	V	$\eta(\lambda)$	Mean	R.M.S	trials
		0.12	6.59×10^3	7.30×10^3	0.118
2363	15	0.23	6.63×10^3	7.35×10^3	0.22
		0.33	6.64×10^3	7.36×10^3	0.33
		0.55	6.58×10^3	7.29×10^3	0.55
		0.12	1.82×10^3	2.07×10^3	0.118
2363	20	0.23	1.83×10^3	2.08×10^3	0.232
		0.33	1.83×10^3	2.08×10^3	0.327
		0.55	1.83×10^3	2.08×10^3	0.55
		0.12	7.35×10^2	8.49×10^2	0.118
2363	25	0.23	7.24×10^2	8.37×10^2	0.23
		0.33	7.27×10^2	8.37×10^2	0.33
		0.55	7.25×10^2	8.37×10^2	0.55

Table 4.2: The mean and R.M.S for distribution of anode electrons for dynode potentials [0,50,100,150,200,250,300].

Figure 4.9: Distribution of anode electrons for dynode potentials:[0,150,300,450,600,750,900],for Table. 4.5.

Figure 4.10: Distribution of anode electrons for dynode potentials:[0,150,300,450,600,750,900] for Table. 4.5.
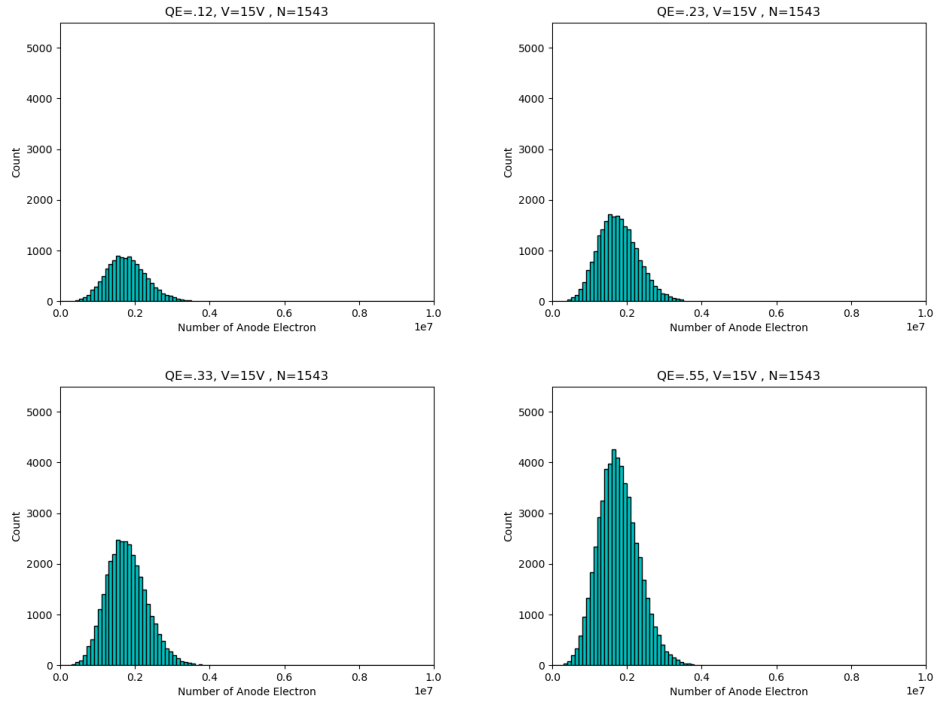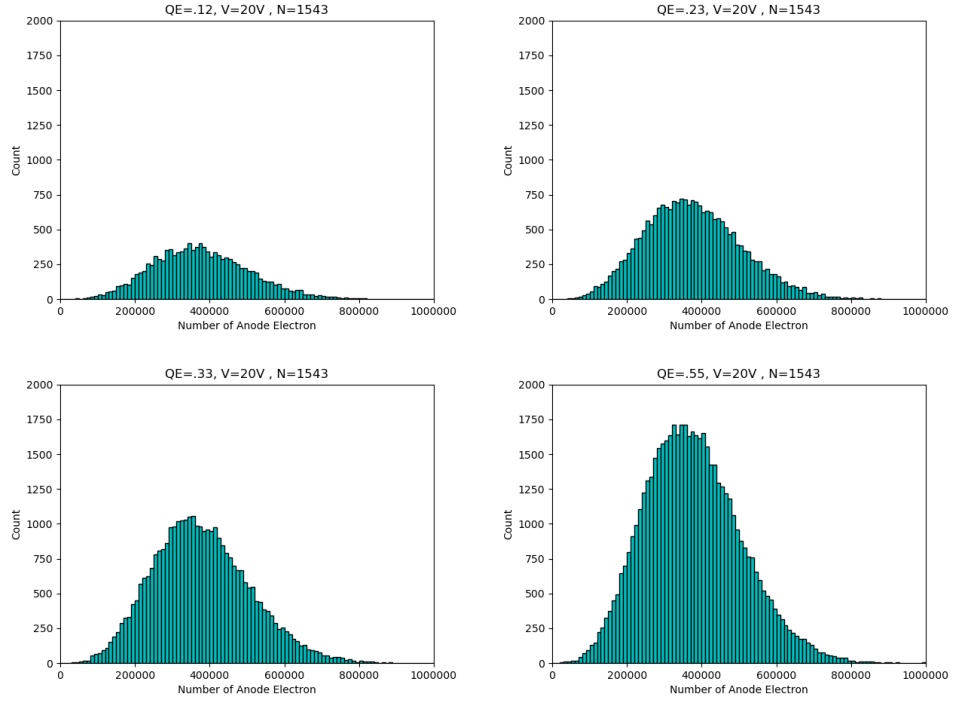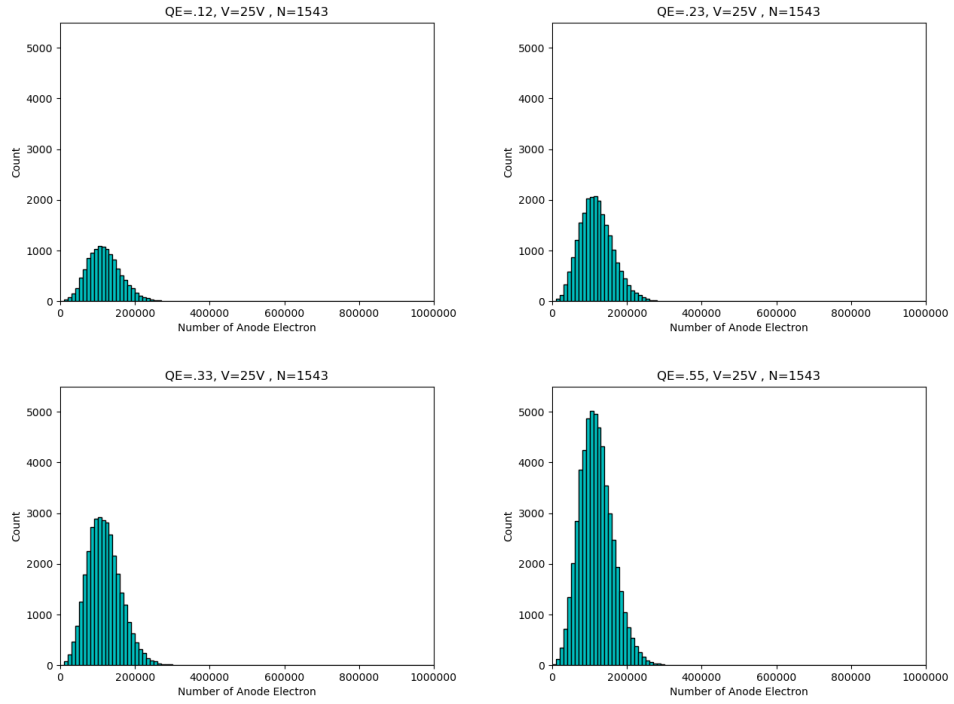
N_γ	V	$\eta(\lambda)$	Mean	R.M.S	trials
1543	15	0.12	6.59×10^3	7.32×10^3	0.12
		0.23	6.62×10^3	7.34×10^3	0.23
		0.33	6.62×10^3	7.35×10^3	0.329
		0.55	6.63×10^3	7.36×10^3	0.55
1543	20	0.12	1.84×10^3	2.10×10^3	0.122
		0.23	1.82×10^3	2.07×10^3	0.22
		0.33	1.83×10^3	2.08×10^3	0.33
		0.55	1.83×10^3	2.07×10^3	0.549
1543	25	0.12	7.35×10^2	8.49×10^2	0.11
		0.23	7.29×10^2	8.42×10^2	0.228
		0.33	7.32×10^2	8.46×10^2	0.32
		0.55	7.26×10^2	8.39×10^2	0.55

Table 4.3: The mean, R.M.S for the distribution of anode electrons for dynode potentials:[0,50,100,150,200,250,300].

Figure 4.11: Distribution of anode electrons for dynode potentials:[0,50,100,150,200,250,300],for Table. 4.2.
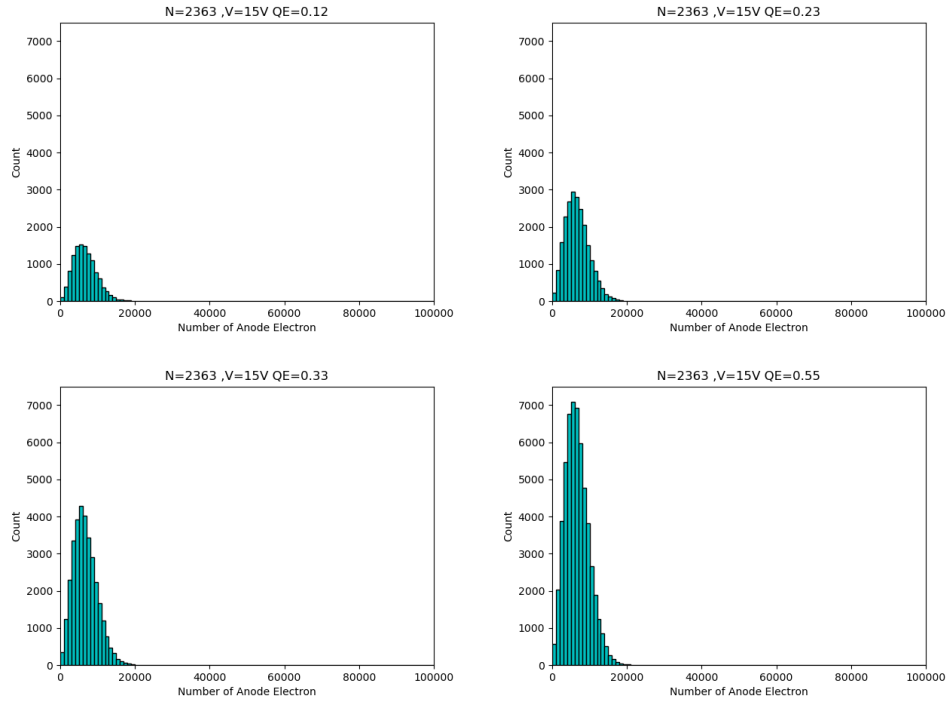

Figure 4.12: Distribution of anode electrons for dynode potentials [0,50,100,150,200,250,300], for Table. 4.2.

Figure 4.13: Distribution of anode electrons for the dynode [0,50,100,150,200,250,300] for table4.2

Figure 4.14: Distribution of anode electrons for dynode potentials [0,50,100,150,200,250,300] for Table. 4.3

N_γ	V	$\eta(\lambda)$	Mean	R.M.S	trials
		0.12	1.76×10^6	1.84×10^6	0.119
2363	15	0.23	1.77×10^6	1.85×10^6	0.23
		0.33	1.77×10^6	1.85×10^6	0.329
		0.55	1.77×10^6	1.85×10^6	0.55
		0.12	3.76×10^5	3.98×10^5	0.118
2363	20	0.23	3.77×10^5	3.98×10^5	0.229
		0.33	3.76×10^5	3.97×10^5	0.32
		0.55	3.77×10^5	3.98×10^5	0.549
		0.12	1.18×10^5	1.26×10^5	0.119
2363	25	0.23	1.17×10^5	1.25×10^5	0.229
		0.33	1.17×10^5	1.25×10^5	0.328
		0.55	1.18×10^5	1.26×10^5	0.55

Table 4.4: The mean and R.M.S for the distribution of anode electrons for dynode potentials [0,150,300,450,600,750,900].
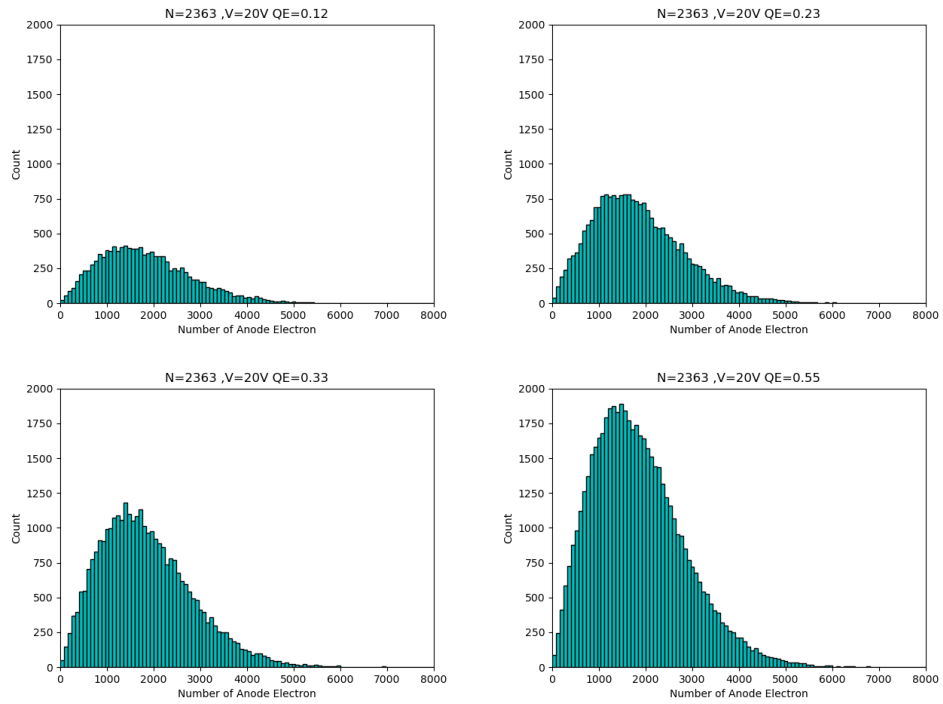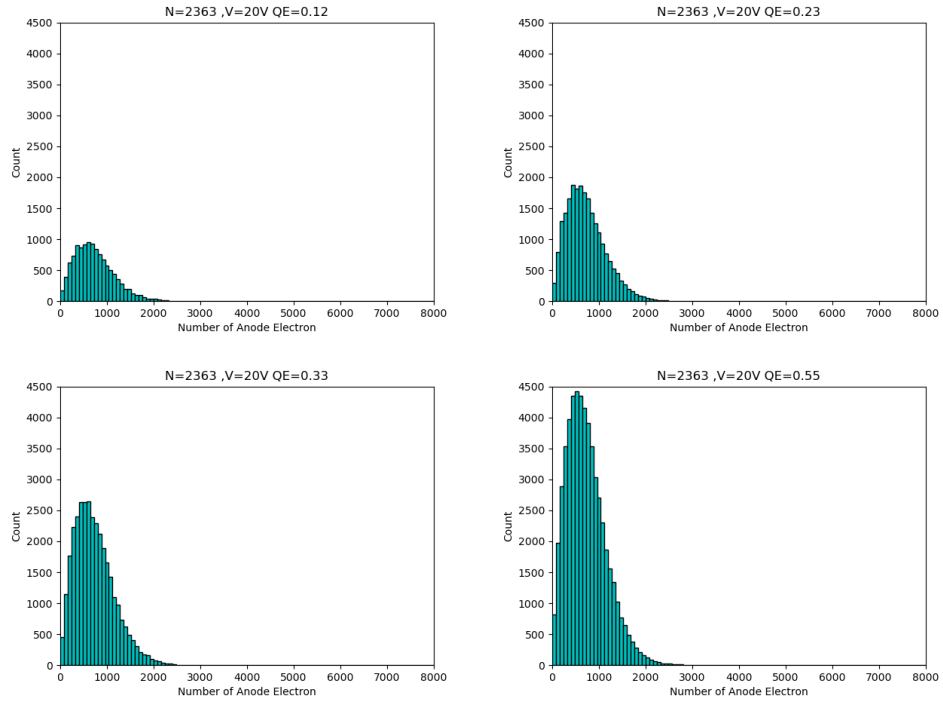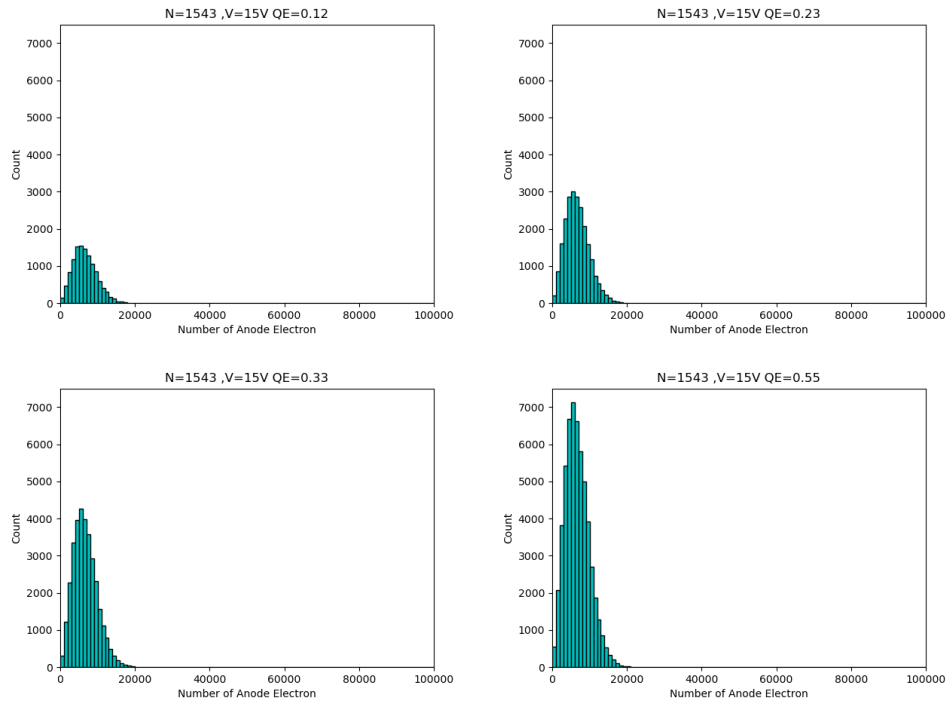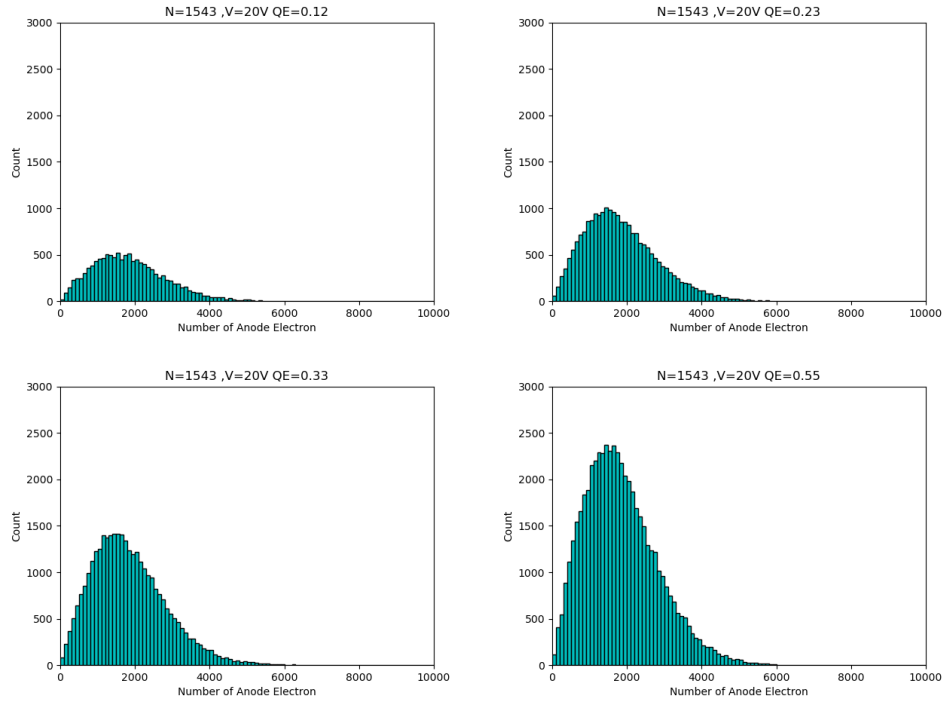
Figure 4.15: Distribution of anode electrons for dynode potentials [0,50,100,150,200,250,300], for Table. 4.3.
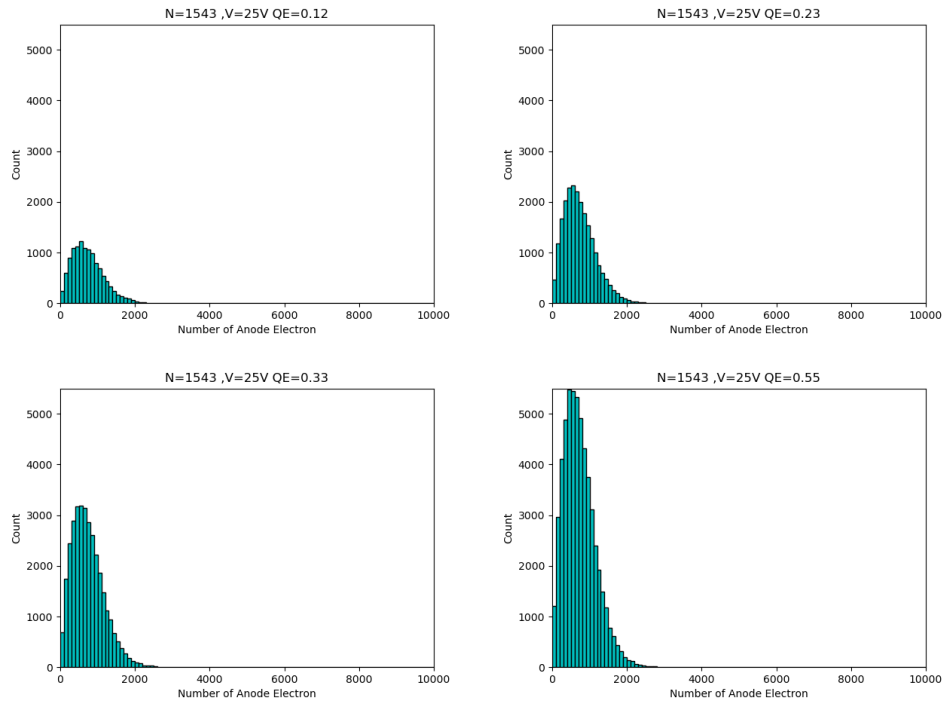

Figure 4.16: Distribution of anode electrons for dynode potentials [0,50,100,150,200,250,300], for Table. 4.3

N_γ	V	$\eta(\lambda)$	Mean	R.M.S	trials
1543	15	0.12	1.76×10^6	1.84×10^6	0.119
		0.23	1.76×10^6	1.84×10^6	0.228
		0.33	1.77×10^6	1.85×10^6	0.329
		0.55	1.76×10^6	1.84×10^6	0.549
1543	20	0.12	3.78×10^5	4.001×10^5	0.122
		0.23	3.76×10^5	3.98×10^5	0.23
		0.33	3.78×10^5	3.99×10^5	0.331
		0.55	3.76×10^5	3.98×10^5	0.551
1543	25	0.12	1.17×10^5	1.26×10^5	0.12
		0.23	1.17×10^5	1.25×10^5	0.229
		0.33	1.17×10^5	1.25×10^5	0.33
		0.55	1.17×10^5	1.25×10^5	0.551

Table 4.5: The mean and R.M.S for the distribution of anode electrons for dynode potentials [0,150,300,450,600,750,900].

No.of dynodes	V	$\eta(\lambda)$	Mean	R.M.S	trials
6			4.43×10^4	4.68×10^4	0.228
7	20	0.23	3.76×10^5	3.97×10^5	0.23
8			3.20×10^6	3.38×10^6	0.228

Table 4.6: The mean and R.M.S for the distribution of anode electrons for different number of dynodes.
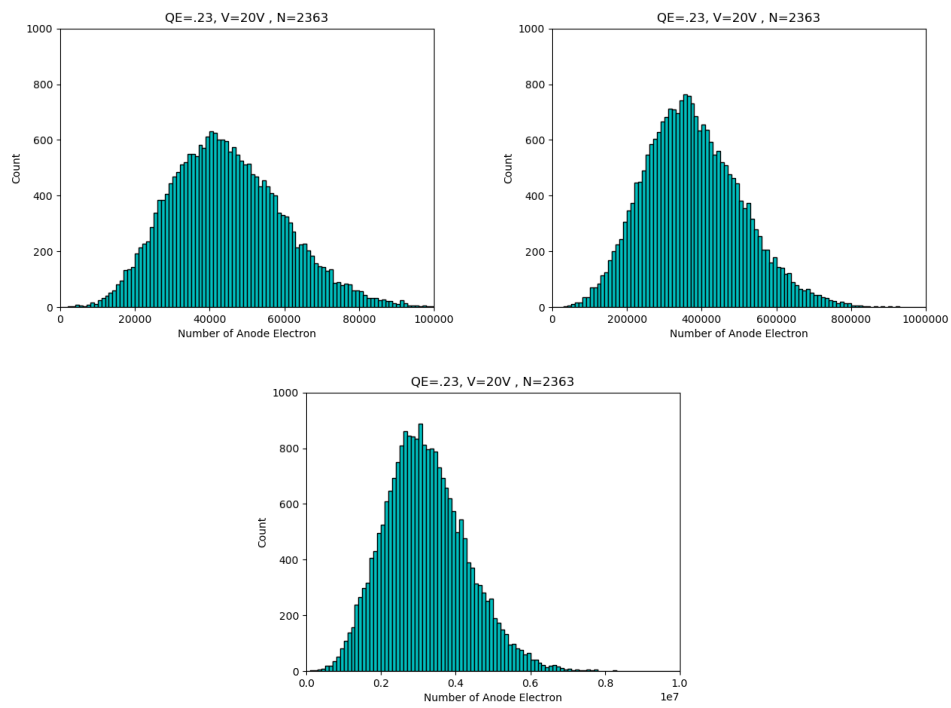
Figure 4.17: Distribution of anode electrons when the number of dynode increased as 6,7 and 8.for Table. 4.6.

Inferences

- The fraction of trails determines what fraction of maximum trials actually produced electrons at the PMT anode. It will be close the the quantum efficiency $\eta_(\lambda)$.

- As seen in the Table. 4.2, mean and R.M.S remains almost the same for all $\eta(\lambda)$ for a fixed number of dynodes and dynode potentials.

- As the applied voltage is increased, the mean and R.M.S decrease. The number of anode electrons produced is independent of N_γ (1543 and 2363) as seen from Tables. 4.2 and 4.3.

- The Tables. 4.4 and 4.5, correspond to the dynode potentials $[0, 150, 300, 350, 400, 650, 900]$. The mean and R.M.S of the distributions remain almost the same for different applied voltage (V) and the different quantum efficiencies.

- As the voltage applied is changed keeping $\eta(\lambda)$ and N_γ the same, we can see a drastic change in the mean and R.M.S. of the distribution.

- The dynode potential has an important role in determining the mean and R.M.S of the distribution i.e comparing Tables. 4.2,4.3,4.4 and 4.5 we can see a drastic change in the mean and R.M.S of the distributions for a decrease in dynode potentials.

We can conclude that as $\eta(\lambda)$ increases for a set of dynode potential, voltage V and N_γ, there is an increase in the peak of the distribution. There is a sharp increase in count according to the no.of anode electrons produced. The number of anode electrons produced decreases and the count increases as the voltage is increased. Table. 4.2 shows that when the number of dynodes is increased, the mean and R.M.S of the distributions increase. The increase in the number of dynodes causes significant increase in the number of electrons reaching the anode, the distribution curves give a clear idea about these.

CHAPTER 5

Summary and future plans

– The basic properties of neutrinos, their sources along with the standard model of elementary particle and some long baseline neutrino experiments were discussed.

– The experimental set up and working of the long baseline neutrino oscillation experiment, T2K including its near and far detector were understood.

– The kinematics of 2–body decay of charged pions to muons and (anti–)muon neutrino was studied in detail. The dependence of neutrino energy on the the parent pion energy and the angle between the neutrino and pion beam in the lab–frame were understood. Expression for relative neutrino flux was also derived.

– Study of variation of anode electron distribution of a PMT with variation in different PMT parameters was performed in chapter 4. The means and R.M.Ss of the anode electron distributions for different configurations were computed, tabulated and plotted. The dependence of this distribution on the applied voltage between the primary electrodes, the potentials and number of dynodes was understood. The distribution was seen to be independent of the quantum efficiency.

– Python codes were written for the simulation studies I performed for off–axis angle and the PMT anode electron variations.

– Future plans - to understand the decrease of neutrino flux with increase in the off–axis angle, to understand the cherenkov emission conditions, calculation of cherenkov angle for different particles in a water cherenkov detector and write codes for these calculations in python.

Bibliography

[1] https://en.wikipedia.org/wiki/Beta$_d ecay/media/File : RaE1.jpg$.

[2] http://hyperphysics.phy-astr.gsu.edu/hbase/particles/cowan.html.

[3] https://www.pngfind.com/pngs/m/556-5569788$_s tandard-model-of-elementary-particles-anti-standard-model.png$.

[4] https://www.google.com/url?sa=iurl=https.

[5] J. N. Bahcall, A. M. Serenelli, and S. Basu, "New solar opacities, abundances, helioseismology, and neutrino fluxes," *The Astrophysical Journal, 621:L85–L88,*, 2005.

[6] U. Katz and C. Spiering, "High-energy neutrino astrophysics: Status and perspectives," *Progress in Particle and Nuclear Physics*, vol. 67, no. 3, pp. 651–704, 2012.

[7] https://www.google.com/imgres?www.researchgate.neturl=httpswww.researchgate.net.

[8] https://encrypted-tbn0.gstatic.com/images?q=tbn:.

[9] https://www.google.com/imgres?q=super.

[10] https://www.google.com/imgres?q=cherenkov

[11] https://www.google.com/url?sa=iurl=httphyperphysics.phy-astr.gsu.edultrans.htmlpsig=.

[12] P. Avery, "Relativistic kinematics 1 and 2," 2015.

[13] Hamanstu, *Photomultiplier Tubes Basics and applications,4th edition.* Hamanstu.

[14] D. Motta and S. Schönert, "Optical properties of bialkali photocathodes," *Nuclear Instruments and Methods in Physics Research Section A: Accelerators, Spectrometers, Detectors and Associated Equipment*, vol. 539, no. 1, pp. 217–235, 2005.

[15] https://www.google.com/url?sa=tsource=webrct=jopi=89978449url=https://psec.uchicago.edu/librar $2ahUKEwiq7Y3p9aiHAxWjb2wGHfeeDS0QFnoECCoQAQusg$ $=$ $AOvVaw1thcVwbgY89g5qXtnO8oWO$.

[16] https://spie.org/images/Graphics/Newsroom/Imported-2016/SPIEPro$_A pril16_p hotomultiplier/kamiok$

[17] D. Perkins, *Particle Astrophysics.* Oxford university Press, 2003.

[18] Y. Suzuki, "Solar neutrinos,"

[19] http://www.math.utah.edu/ beebe/talks/2015/qtm/pdf/pauli-1930-ltc.pdf.

[20] G. Rajasekaran, "Fermi and the theory of weak interactions," *Resonance (Indian Academy of Sciences, Bangalore), Vol 19, No 1, p18-44*, 2014 January.

[21] E. Fermi, "An attempt to a β rays theory," *Nuova Serie N. 1, Pag. 1–20*, 1934.

[22] R. G. Arns, "Detecting the neutrino," *Phys. perspect. 3 (2001) 314–334*, 2001.

[23] https://d3i71xaburhd42.cloudfront.net/3a60b4f8d12f0a8e609ee90baca3ce2c9a9379fd/250px/10-Figure5-1.png.

[24] https://www.google.com/url?sa=iurl=https

[25] R. Oerter, ". the theory of almost everything: The standard model, the unsung triumph of modern physics," 2006.

[26] S. N. Bose, "Planck's law and the hypothesis of light quanta," *Zeitschrift für Physik*, 1924.

[27] E. Fermi, "Sulla quantizzazione del gas perfetto monoatomico rendiconti lincei, (in italian). 3: 145–9., translated as zannoni, alberto (1999-12-14). "on the quantization of the monoatomic ideal gas". arxiv:cond-mat/9912229," *arXiv:cond-mat/9912229*, 1926.

[28] P. A. M. Dirac, "On the theory of quantum mechanics," *Proceedings of the Royal Society A. 112 (762)*, 1926.

[29] R. L. Workman and Others, "Review of Particle Physics," *PTEP*, vol. 2022, p. 083C01, 2022.

[30] https://www.nobelprize.org/prizes/physics/2015/press-release/.

[31] https://www.forbes.com/sites/startswithabang/2016/09/09/cosmic-neutrinos-detected-confirming-the-big-bangs-last-great-prediction.

[32] https://www.nobelprize.org/prizes/physics/2002/summary/.

[33] C. W. K. Carlo Giunti, *Fundamentals of Neutrino Physics and Astrophysics.* Oxford University Press, 2007.

[34] C. W. K. Carlo Giunti, *Fundamentals of Neutrino Physics and Astrophysics.* Oxford University Press, 2007.

[35] O. Pisanti, "Astrophysical neutrinos: theory," *arXiv:1906.12258v1 [astro-ph.CO]*, 2019.

[36] TheIceCubeCollaboration, "Observationofastrophysicalneutrinosinsixyears oficecube-data," *PoS(ICRC2017)981*, 2019.

[37] T. M. Undagoiti, "Neutrino physics: Theory and experiment (ss2021) neutrino sources and neutrino detectors," *Max-Planck-Institut f¨ur Kernphysik, Saupfercheckweg 1, 69117 Heidelberg, Germany.*

[38] X. Qian and J.-C. Peng, "Physics with Reactor Neutrinos," *Rept. Prog. Phys.*, vol. 82, no. 3, p. 036201, 2019.

[39] https://www.google.com/url?sa=tsource=webrct=jopi=89978449url=https://arxiv.org/html/2.

[40] A. Ajmi, "Latest Results from the T2K and NOvA Experiments," *PoS*, vol. HQL2023, p. 024, 2024.

[41] A. Habig, "The NOvA Experiment," *Nucl. Phys. B Proc. Suppl.*, vol. 229-232, pp. 460–460, 2012.

[42] A. Bellerive, J. R. Klein, A. B. McDonald, A. J. Noble, and A. W. P. Poon, "The Sudbury Neutrino Observatory," *Nucl. Phys. B*, vol. 908, pp. 30–51, 2016.

[43] Y. F. et al. (Super-Kamiokande Collaboration), "Evidence for oscillation of atmospheric neutrinos," *Phys. Rev. Lett. 81, 1562 (1998) – Published 24 August 1998*, 1998.

[44] S. Floerchinger and J.-M. Schwindt, "Neutrino flavor-mass uncertainty relations and an entanglement-assisted determination of the PMNS matrix," *Phys. Rev. D*, vol. 102, no. 9, p. 093001, 2020.

[45] M. H. Ahn *et al.*, "Measurement of Neutrino Oscillation by the K2K Experiment," *Phys. Rev. D*, vol. 74, p. 072003, 2006.

[46] J. Evans, "The MINOS Experiment: Results and Prospects," *Adv. High Energy Phys.*, vol. 2013, p. 182537, 2013.

[47] Y. Itow, "Construction status and prospects of the Hyper-Kamiokande project," *PoS*, vol. ICRC2021, p. 1192, 2021.

[48] B. Abi *et al.*, "Prospects for beyond the Standard Model physics searches at the Deep Underground Neutrino Experiment," *Eur. Phys. J. C*, vol. 81, no. 4, p. 322, 2021.

[49] https://www.google.com/url?sa=tsource=webrct=jopi=89978449url=https://t2k-experiment.org/publications/ved=2ahUKEwjTz5btlqmHAxWa2DgGHR9WBUQQFnoECA8QAQusg=

[50] K. Aoki *et al.*, "Extension of the J-PARC Hadron Experimental Facility: Third White Paper," 10 2021.

[51] Y. Fukuda *et al.*, "The Super-Kamiokande detector," *Nucl. Instrum. Meth. A*, vol. 501, pp. 418–462, 2003.

[52] https://www.google.com/imgres?q=T2K.

[53] K. Abe *et al.*, "Constraint on the matter–antimatter symmetry-violating phase in neutrino oscillations," *Nature*, vol. 580, no. 7803, pp. 339–344, 2020. [Erratum: Nature 583, E16 (2020)].

[54] K. Abe *et al.*, "Precise Measurement of the Neutrino Mixing Parameter θ_{23} from Muon Neutrino Disappearance in an Off-Axis Beam," *Phys. Rev. Lett.*, vol. 112, no. 18, p. 181801, 2014.

[55] Y. Fukuda *et al.*, "Evidence for oscillation of atmospheric neutrinos," *Phys. Rev. Lett.*, vol. 81, pp. 1562–1567, 1998.

[56] K. A. et al., "Solar neutrino measurements using the full data period of super-kamiokande-iv,"

[57] D. Griffiths, *Introduction to Elementary Particles*. Wiley - VCH, 2008.

[58] C. I. U. P. V. e. P. V. P. Jean-Michel Levy, Laboratoire de Physique Nucl´eaire et de Hautes Energies, "Kinematics of an off-axis neutrino beam," *arXiv:1005.0574v2 (hep-ex)*, 2010.

[59] R. Sahoo, "Relativistic kinematics," *Lecture delivered in IX SERC School on Experimental High Energy Physics, IIT Madras*, 2013.

[60] R. M. Barnett *et al.*, "Review of particle physics. Particle Data Group," *Phys. Rev. D*, vol. 54, no. 1, pp. 1–720, 1996.

[61] K. T. McDonald, "An off-axis neutrino beam," *Joseph Henry Laboratories, Princeton University,NJ08544*, 2019, June 5.

[62] S. Aiello *et al.*, "Probing invisible neutrino decay with KM3NeT/ORCA," *JHEP*, vol. 04, p. 090, 2023.

[63] Q. R. Ahmad *et al.*, "Direct evidence for neutrino flavor transformation from neutral current interactions in the Sudbury Neutrino Observatory," *Phys. Rev. Lett.*, vol. 89, p. 011301, 2002.

[64] M. G. Aartsen *et al.*, "The IceCube Neutrino Observatory: Instrumentation and Online Systems," *JINST*, vol. 12, no. 03, p. P03012, 2017. [Erratum: JINST 19, E05001 (2024)].

[65] S. Jetter, D. Dwyer, W.-Q. Jiang, D.-W. Liu, Y.-F. Wang, Z.-M. Wang, and L.-J. Wen, "PMT waveform modeling at the Daya Bay experiment," *Chin. Phys. C*, vol. 36, pp. 733–741, 2012.

[66] S. D. e. a. Willger, "Characterization of the pmt gene family in cryptococcus neoformans.," *PloS one vol. 4,7 e6321. 27 Jul. 2009, doi:10.1371/journal.pone.0006321*, 2009.

[67] H. Hertz, ""ueber einen einfluss des ultravioletten lichtes auf die electrische entladung"," *Annalen der Physik. 267*, 1887.

[68] W.Hallwachs, """ueber den einfluss des lichtes auf electrostatisch geladene körper," 301–312," *Annalen der Physik und Chemie*, 1889.

[69] J.Elster and H.Geitel *Annalen der Physik und Chemie*, 1888.

[70] A. Einstein, ""Über einen die erzeugung und verwandlung des lichtes betreffenden heuristischen gesichtspunkt"," *Annalen der Physik und Chemie*, 1905.

[71] https://www.nobelprize.org/prizes/physics/1921/summary/.

[72] w.R. Leo, *Techniques for nuclear and Particle Physics experiment.* Springer Verlag, 1987.

[73] https://www.google.com/url?sa=tsource=webrct=jopi=89978449url=https://www.hamamatsu.com/j sensors/pmt.htmlved=2ahUKEwjgx72r-qiHAxVNTmwGHahZDzkQFnoECDsQAQusg=AOvVaw16KG

[74] https://www.google.com/url?sa=tsource=webrct=jopi=89978449url=https://accelconf.web.cern.ch/pa KiHAxU9SWwGHde$_B$xkQFnoECCgQAQusg$\quad = \quad AOvVaw35R6lIdN \quad - DeuyzvRVsm5Ag$.

[75] https://www.google.com/url?sa=tsource=webrct=jopi=89978449url=http://hep.ucsb.edu/people/hnn $02_20inch_superKmain.pdf ved = 2ahUKEwiswKSP96iHAxXGW2wGHaqsA8QQFnoECBQQAQus AOvVaw0vDqttCWBk9BoZyEbXlHJb$.

[76] P. T. D. Neutrinos, "Chris warner," 2016.

[77] M. Lafleur, P. Hinrichsen, P. Landry, and R. Moore, "The poisson distribution," *The Physics Teacher*, vol. 10, pp. 314–321, 09 1972.

[78] A. Adekitan, "Monte carlo simulation," 09 2014.

[79] https://cmps-people.ok.ubc.ca/jbobowsk/Python/html/Jupyter